

Microemulsions with sticker polymers as efficiency boosters investigated by SANS

von

Martin Brodeck

Diplomarbeit der PHYSIK
vorgelegt der

**Fakultät für Mathematik, Informatik und Naturwissenschaften
der RWTH Aachen**

im August 2006

angefertigt im

Institut für Festkörperforschung (IFF) am Forschungszentrum Jülich

Prof. Dr. Thomas Brückel, Prof. Dr. Dieter Richter

Contents

1	Introduction	5
2	Theory of microemulsions	7
2.1	Characterization of microemulsions	7
2.2	Curvature energy	8
2.2.1	Curvature of the membrane	8
2.2.2	The Helfrich model	9
2.2.3	The curvature of bicontinuous microemulsions	11
2.3	The polymer boosting effect	12
2.3.1	Addition of diblock copolymers	13
2.3.2	Addition of sticker polymers	16
3	Phase diagram studies	18
3.1	The $T(\gamma)$ phase diagram	18
3.1.1	Analysis of the phase diagrams	20
3.2	Experimental determination of phase diagrams	21
3.3	Interpretation	22
4	Small angle neutron scattering	24
4.1	General aspects	24
4.2	Experimental details	26
4.2.1	Setup	26
4.2.2	Corrections	28
4.3	Scattering on microemulsions	31
4.3.1	The Gaussian Random Field approximation	31
4.3.2	The Ginzburg-Landau model	32
5	Materials	34
5.1	Synthesis and characterization of the anionic sticker polymers	34
5.2	Characterization of the ionic sticker polymers	37

6	Experiments	38
6.1	Phase diagrams	38
6.1.1	Nonionic sticker polymers	38
6.1.2	Ionic sticker polymers	41
6.1.3	Investigation of the fish-tail points	45
6.2	SANS measurements	46
6.2.1	Sample preparation and measurement	46
6.2.2	Discussion of scattering functions	46
7	Discussion	52
7.1	Efficiency boosting	52
7.2	Spontaneous curvature	55
7.3	Bending rigidity	57
8	Summary and conclusions	64
9	Bibliography	67

Chapter 1

Introduction

The polymer boosting effect is induced by amphiphilic diblock copolymers that are added to microemulsions consisting of water, oil and an anionic surfactant. The efficiency of these systems is greatly increased reducing the minimum amount of surfactant necessary to emulsify all available oil and water [1, 2]. This work focuses on the efficiency-boosting effect of sticker polymers in microemulsions. If these polymers function equally well they present a cost-effective alternative to the chemically more complicated diblock copolymers and might make their way into various industrial applications.

Water is a polar liquid which does not mix with hydrophobic substances as oil. Combining both with a surfactant, they will form a thermodynamically stable microemulsion where the oil and water domains are separated by an amphiphilic surfactant film. Using equal amounts of oil and water, these domains with a size of several hundred Angstroms form bicontinuous phases. The physical properties can be described by the Helfrich model [3], which assumes that the surface elasticity dominates the free energy of the system. Three thermodynamic parameters, the bending moduli κ , $\bar{\kappa}$ and the spontaneous curvature c_0 , are introduced to connect the free energy with the mean curvature and the Gaussian curvature.

The addition of diblock copolymers as a fourth component to bicontinuous microemulsions was first investigated by H. Endo, B. Jacobs and co-workers [1, 2]. They found that with the addition of these polymers less surfactant was necessary to form a one-phase microemulsion. This feature is called the boosting effect. The structure of diblock copolymers is similar to that of the surfactant molecules, only the length of the hydrophilic and hydrophobic group is increased. The explanation to the boosting effect was given by H. Endo with small angle neutron scattering (SANS) measurements [2]. Using contrast variation methods, he found that the polymer is anchored to the membrane. The entropic force of the polymer chains increases the rigidity of the interface and allows for larger domain structures. Thus a better surface to volume fraction is achieved.

We use two methods to investigate microemulsions. In phase diagram measurements we visually observe the state of the system depending on changes in the amount of surfactant and temperature. This lets us quantify the boosting effect of the investigated polymer. Following an established procedure, the emulsification failure boundary is connected with changes of $\bar{\kappa}$. In contrast to this, SANS experiments with bulk contrast (water/oil) allow us to study the mesoscopic structure of water and oil domains. The scattering data can be described by the Teubner-Strey formula [4] and yields the domain size d and the correlation length ξ . Using the Gaussian random field model it is possible to connect these two structural parameters with κ . Therefore SANS offers the possibility to directly measure the bending rigidity, which can be compared with the saddle-splay modulus obtained from phase diagram measurements.

Sticker polymers introduce a new feature evoked by their asymmetric structure. They are only able to influence the membrane from one side and therefore cause a change of the spontaneous curvature c_0 . Strey [5] has connected this change with a shift of the phase inversion temperature \tilde{T} which is accessible from phase diagram measurements.

We have investigated three non-ionic and two ionic sticker polymers. The non-ionic polymers are chemically similar to the used surfactant, C₁₀E₄. A short hydrophobic sticker consisting of several carbon atoms allows to anchor the otherwise hydrophilic polymer to the membrane. The hydrophilic part comes in a monofunctional and a bifunctional configuration: one single polymer chain consisting of 90 ethylene oxide groups, and two of these chains linked together at the short sticker. The ionic polymers carry a carboxyl group (COOH) as sticker. It is necessary to add NaOH to the system to allow this sticker to dissociate in the water domains. Polybutadiene and poly(t-butyl acrylate) constitute the hydrophobic part of these polymers.

Apart from ease of production and cost-effectiveness sticker polymers offer significant advantages. The possibility to choose the preferred solubility allows a placement of the polymer inside or outside in droplet microemulsions. Their high solubility selectively in water or oil makes them interesting for applications ranging from cleaning agents to cosmetics. All these advantages bring sticker polymers closer to applications than diblock copolymers have already been.

Chapter 2

Theory of microemulsions

Microemulsions consist of two immiscible components (usually water and oil), a surfactant and possibly other components such as polymers. Without any additives oil will not be able to dissolve in water due to the polarity of water molecules. Water is a hydrophilic (polar) and oil is a hydrophobic (non-polar) liquid. Mixing the two components will soon result in a phase separation where the lighter oil floats on top of the water phase. Adding an amphiphilic surfactant, which is composed of hydrophilic and hydrophobic structural entities, will microscopically form an interface between local water and oil domains. The interfacial tension is drastically decreased by the surfactant. The size of these domains lies in the range of nanometers.

2.1 Characterization of microemulsions

The structure of the oil and water domains define the behavior of the system. This structure depends on the amount of surfactant available to form the microemulsion. Ψ describes the membrane volume fraction and is defined as:

$$\Psi = \frac{aS}{V} = \frac{a}{\lambda} \quad (2.1)$$

where a is the size (length) of the surfactant molecules, S stands for the surface of the membrane and V is the volume of the system. The volume to surface ratio V/S can also be expressed by λ . Very low amounts of surfactant will just be solved in oil and water and no structure is formed. As the surfactant concentration crosses the CMC-barrier (critical micelle concentration), spherical, cylindrical or ellipsoidal micelles can form. Also bicontinuous sponge-like phases appear. At high amounts of the amphiphile lamellar structures start to appear. In this case the system is composed of alternating

layers of oil and water.

For an easier handling in the laboratory we usually work with mass ratios instead of volume fractions. The composition of a system is therefore described by the water to oil mass ratio α and the relative amount of surfactant γ :

$$\alpha = \frac{m_{oil}}{m_{oil} + m_{water}} \quad (2.2)$$

$$\gamma = \frac{m_{surfactant}}{m_{surfactant} + m_{oil} + m_{water}} \quad (2.3)$$

The corresponding water to oil volume fraction is Φ :

$$\Phi = \frac{V_{oil}}{V_{oil} + V_{water}} \quad (2.4)$$

Throughout this work we will discuss symmetric microemulsions with $\Phi = 0.5$.

2.2 Curvature energy

The behavior of microemulsions is primarily influenced by the curvature energy of the amphiphilic film. To model the physical properties of the system we describe the bending energy of this film and introduce fundamental parameters such as the bending rigidity κ , the saddle-splay modulus $\bar{\kappa}$ and the spontaneous curvature c_0 . This can be achieved with the *Helfrich model* [3]. To apply this model we first have to define the local curvature of an interface.

2.2.1 Curvature of the membrane

To describe the curvature and topology of the film we introduce the two main curvatures $c_1 = R_1^{-1}$ and $c_2 = R_2^{-1}$ (Figure 2.1). c_i is by definition positive for a curvature towards the oil domains and negative for a curvature around the water domains. The mean curvature H and the Gaussian curvature K are then defined as:

$$H = \frac{1}{2}(c_1 + c_2) \quad (2.5)$$

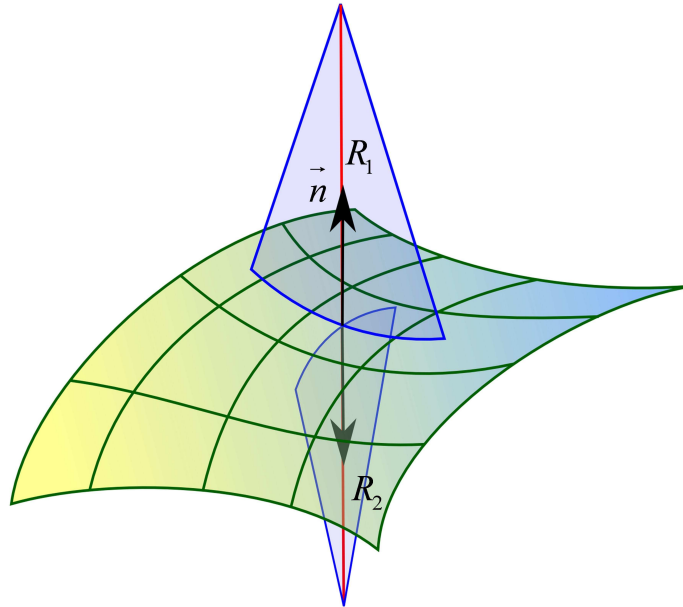


Figure 2.1: Every point on the interface can be described by the radii of two perpendicular circles that reflect to local curvature of the given point. In the case of $R_1 = -R_2$ a saddle-splay formation is found.

$$K = c_1 c_2 \quad (2.6)$$

Different structures can now be identified with different curvatures c_i :

- spherical shapes: $c_1 = c_2$ and $H = r^{-1}$
- cylindrical shapes: $c_1 = 0, c_2 = r_2^{-1}$ and $H = \frac{1}{2}c_2$
- saddle-splay form: $c_1 = -c_2$ and $H = 0$
- lamellar structure: $c_1 = c_2 = 0$ and $H = 0, K = 0$

2.2.2 The Helfrich model

Now that we have a mathematical description of the membrane curvature we can introduce the Helfrich model. The Helfrich model assumes that the interface dominates the

free energy of the microemulsion. The bending energy of a bicontinuous system is then described by the Hamiltonian:

$$F = \int dS [2\kappa(H - c_0)^2 + \bar{\kappa}c_1c_2] \quad (2.7)$$

The integral is summed over the whole interface S . κ and $\bar{\kappa}$ describe the bending rigidity and the saddle-splay modulus of the membrane. κ can be interpreted as the energy needed to bend the interface away from the spontaneous curvature c_0 . The spontaneous curvature represents the *natural* bending of the interface without external influence. This approach explains the formation of spherical and lammellar structures, whereas saddle-splay formations are not possible.

Starting from the lamellar phase and including the effect of thermal fluctuations into the Helfrich model makes it possible to explain the formation of bicontinuous microemulsions. These thermal fluctuations will locally cause a variation of the mean curvature from its average value $H = 0$ and create passages between the lamellae. These fluctuations are included by renormalizing the rigidities as follows:

$$\kappa_R(\lambda) = \kappa - \alpha \frac{k_B T}{4\pi} \ln\left(\frac{\lambda}{a}\right) \quad (2.8)$$

$$\bar{\kappa}_R(\lambda) = \bar{\kappa} - \bar{\alpha} \frac{k_B T}{4\pi} \ln\left(\frac{\lambda}{a}\right) \quad (2.9)$$

Field-theoretic calculations yield the values $\alpha = 3$ and $\bar{\alpha} = -10/3$ [6]. a is the size of the surfactant molecules. The logarithmic renormalization is cut off at length scales of the average domain size of microemulsions. With (2.1) and $\bar{\kappa}_R(\lambda/a) = 0$ at the fish-tail point as Morse proposed [7] we can now write

$$\ln(\Psi/\Psi_0) = \frac{4\pi}{\bar{\alpha}} \frac{\bar{\kappa}}{k_B T} \quad (2.10)$$

$\Psi_0 \approx 1$ is a correction factor induced by the uncertainty of the surfactant molecule size a . With equation 2.10) we have established a relation between the thermodynamical parameter $\bar{\kappa}$ and the macroscopic property of the surfactant content Ψ .

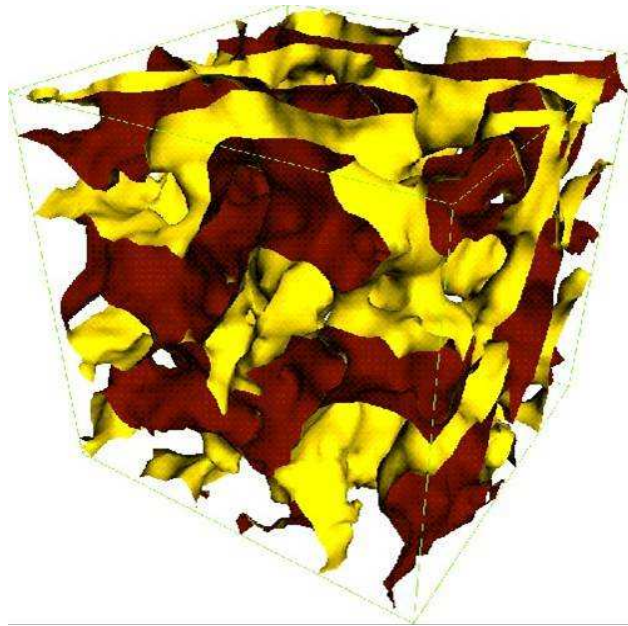


Figure 2.2: Structure of a system in sponge phase. The yellow and red sides of the interface represent the water and oil domains.

2.2.3 The curvature of bicontinuous microemulsions

With the definition of the Helfrich free energy (2.7) we can now take a look at formations of interfaces which minimize the curvature energy. For membranes without a spontaneous curvature ($c_0 = 0$) and saddle-splay modulus $\bar{\kappa} = 0$ the energy is minimized for surfaces which have $\langle H \rangle = 0$ [8]. These surfaces are called *minimal surfaces*. Ternary systems consisting of water, oil and surfactant have stable phases at the phase-inversion temperature \tilde{T} ($c_0 = 0$ at \tilde{T}). These phases are called microemulsions which are isotropic, homogeneous and thermodynamically stable. They consist of a network of water and oil channels that are curved around each other and are separated by the surfactant monolayer. Figure 2.2 shows the microscopic structure of a microemulsion in the so called sponge-phase.

The temperature dependence of the curvature

Strey [5] was able to show with small angle neutron scattering that the mean curvature H in microemulsions depends linearly on the temperature of the system for non-ionic surfactants. A schematic sketch of this observation can be found in Figure 2.3. At the phase-inversion temperature \tilde{T} the mean curvature of the system is $\langle H \rangle = 0$. In this case

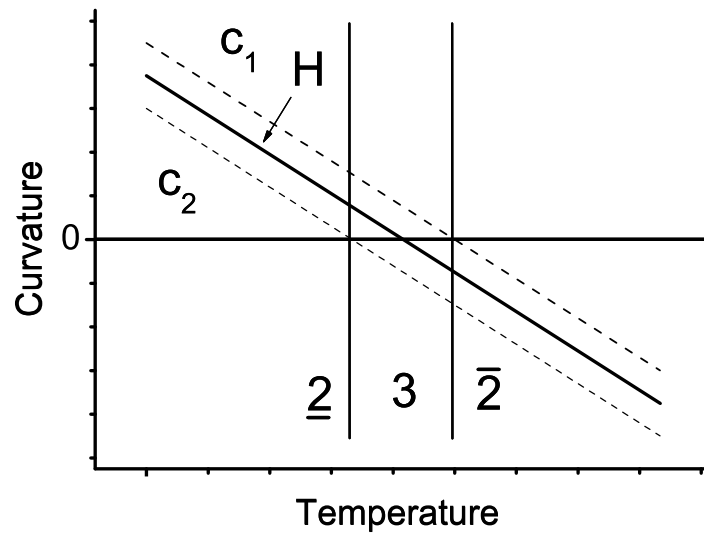


Figure 2.3: Sketch of the principal curvatures c_1 and c_2 and the mean curvature $\langle H \rangle$ as a function of temperature for non-ionic surfactant.

$c_1 = -c_2$ and a saddle-splay structure is expected. Once the two principal curvatures c_1 and c_2 have the same sign, spherical micelles start to form. A closer investigation of this behavior can be found in chapter 3, where the phase behavior of microemulsions is discussed.

2.3 The polymer boosting effect

Up to this point we have only discussed microemulsions with the three components water, oil and surfactant. In 1999 it was found that the addition of diblock copolymers to a microemulsion showed an increased efficiency of the system [1]. Therefore we will first discuss the behavior of diblock copolymers at the interface. These aspects will later be applied to sticker polymers.

To measure the amount of polymer in the system we introduce δ as the mass ratio of polymer to surfactant plus polymer:

$$\delta = \frac{m_{polymer}}{m_{surfactant} + m_{polymer}} \quad (2.11)$$

This way it is easier to compare different membrane to volume fractions since the number of polymers per membrane area stays constant for a fixed value of δ . The surfactant ratio γ is now defined as:

$$\gamma = \frac{m_{surfactant} + m_{polymer}}{m_{surfactant} + m_{oil} + m_{water} + m_{polymer}} \quad (2.12)$$

2.3.1 Addition of diblock copolymers

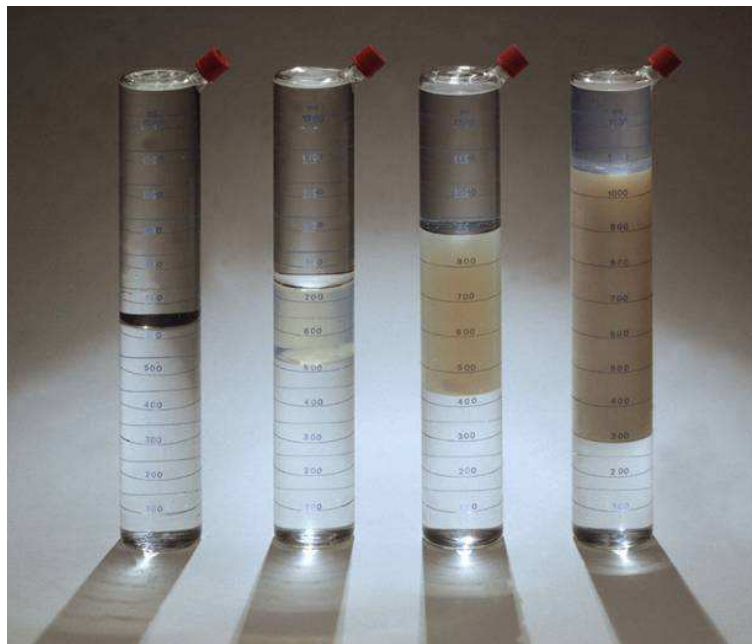


Figure 2.4: Visual demonstration of the polymer boosting effect: The left cylinder is filled with equal volumes of oil and water. Surfactant was added to the system which creates a microemulsion in the middle (second cylinder). The third and fourth cylinder show the same system with the addition of tiny amounts of polymer (0.5wt% and 1.0wt% of the total mass).

The boosting effect was first discovered for diblock copolymers. These amphiphilic polymers consist of a hydrophobic Poly(ethylene-propylene) (PEP) block and a hydrophilic Poly(ethylenoxide) (PEO) block. Adding only small amounts of polymer into a microemulsion dramatically increases the efficiency of the system as can be seen in Figure 2.4. Larger volumes of water and oil can be solubilized with the same amount of surfactant γ . A qualitative analysis of the effect can be found in chapter 6.1.1. Figure 2.4 also shows that the microemulsion becomes nontransparent with increased polymer

amount. This is an indication of an increase of the domain size since light will be scattered as the size of the water and oil domains reach the wavelength of light. At this point we want to take a look at the behavior of the polymer in the system.

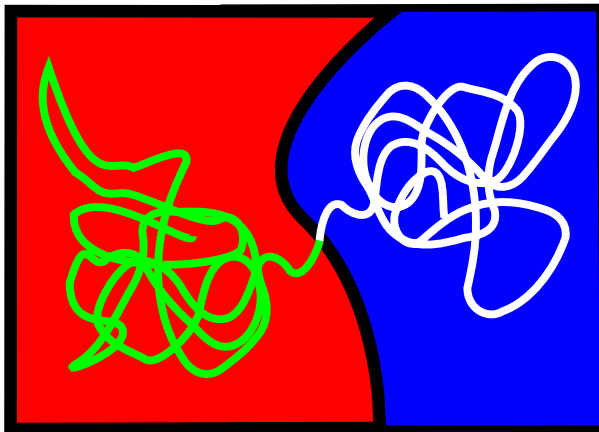


Figure 2.5: Schematic drawing of a diblock copolymer attached to the interface between oil (left) and water (right) domains.

When added to the microemulsion the polymer will attach to the interface between the water and oil domains with its hydrophilic block in water and the hydrophobic block in oil (Figure 2.5). This has been studied with neutron scattering by Hitoshi and Endo using contrast variation methods [2]. Since the chain itself is repelled by the membrane it will form a coil above the interface. A quantity that describes the size of a polymer is the end-to-end distance R_{ee} . R_{ee} is defined as the average distance between the two ends of the polymer chain in coil formation and is proportional to the number N of monomers to the power of ν :

$$R_{ee} \sim N^\nu \quad (2.13)$$

For ideal chains $\nu = 1/2$. We define two end-to-end distances for diblock copolymers: R_w is the end-to-end distance of the hydrophilic block, R_o the end-to-end distance of the hydrophobic block. If there is none or little interaction between different polymer branches, we speak of the “mushroom regime”. When the density of the polymer at the interface, σ , is high enough for a penetration of the polymer coils, the “brush regime” is reached. At this state, the distance between two anchor points gets as small as the end-to-end distance of the polymers. For this work only the “mushroom regime” is of interest since our concentrations were far below the condition for brush regimes ($\sigma R_w^2 \geq 1$; $\sigma R_o^2 \geq 1$).

The strong influence of the amphiphilic polymer can be explained by the membrane

curvature model. Hiergeist and Lipowsky have calculated the change of the bending rigidity κ and the saddle-splay modulus $\bar{\kappa}$ induced by polymers at the interface [9].

$$\kappa_{eff} = \kappa + k_B T \frac{1 + \pi/2}{12} \sigma (R_o^2 + R_w^2) \quad (2.14)$$

$$\bar{\kappa}_{eff} = \bar{\kappa} - k_B T \frac{1}{6} \sigma (R_o^2 + R_w^2) \quad (2.15)$$

σ is the grafting density of the polymer and defined as

$$\sigma = \rho_D a N_A M_W^{-1} \frac{\delta}{1 - \delta} \quad (2.16)$$

ρ_D is the density of the polymer, a the thickness of the membrane, N_A the Avogadro's number, M_W the molecular weight of the polymer chain and δ the volume fraction of the polymer with respect to the total amphiphile (compare eq. (2.11)). σ counts the number of polymers per membrane-area.

(2.14) and (2.15) are only valid in the mushroom regime. The bending rigidity κ increases linearly with the polymer amount whereas the saddle-splay modulus $\bar{\kappa}$ decreases. This behavior can be understood from the entropy loss of the polymer since the available configurations are limited by the existence of the membrane. Fluctuations of the membrane are suppressed and make the interface smoother and at the same time a better surface to volume fraction is achieved. The polymers also disfavor saddle-splay configurations, which has been explained by Milner and Witten [10]. With (2.10) and (2.15) we get a connection between the scaled polymer density and the minimum amount of surfactant needed to solubilize all available water and oil:

$$\ln(\Psi) = \ln(\Psi_0) - \frac{\pi}{5} \sigma (R_w^2 + R_o^2) \quad (2.17)$$

Ψ_0 is the surfactant volume fraction of the fish-tail point without the addition of polymer. (2.17) explains the strong influence of the polymers. Even though κ and $\bar{\kappa}$ are changed only slightly by a fraction of $k_B T$, a macroscopic effect is induced due to the exponential dependence.

Eisenriegler *et al.* [11] have described the influence of the polymers on the spontaneous curvature c_0 as

$$c_{0,eff} = c_0(T) + \frac{1}{4} \sqrt{\frac{\pi}{6}} \frac{k_B T}{\kappa_R} \sigma (R_w - R_o) \quad (2.18)$$

(2.18) states that the addition of **symmetric** diblock copolymers (which means same end-to-end distances on both sides of the membrane, $R_w = R_o$) does not change c_0 , which was confirmed by phase diagram measurements [2]. Adding diblock copolymers with different end-to-end distances of the hydrophilic and the hydrophobic chain will favor a curvature towards the domain with the smaller polymer.

2.3.2 Addition of sticker polymers

Sticker polymers are nothing but diblock copolymers in which the hydrophobic block is missing. Instead, a short sticker of several carbon atoms takes the role of anchoring the polymer in the interface. The length of this sticker is of great importance: If the sticker is not long enough, it will not be able to attach the polymer to the interface. This question will be discussed later (chapter 6.1.1). The hydrophilic chain will try to pull the polymer out of the interface because of the entropic force exerted on the sticker, at the same time the hydrophobic group will try to stay inside the oil domain due to the enthalpic force.

The short sticker obviously shows no chain-like behavior. The influence on the membrane is limited to the effects of the hydrophilic block, which is mathematically expressed by setting the end-to-end distance in oil to $R_o = 0$. The complete description of κ and $\bar{\kappa}$ including renormalization and the addition of a sticker polymers is now:

$$\kappa_R = \kappa_0 \quad (2.19)$$

$$+ \alpha \frac{k_B T}{4\pi} \ln(\Psi)$$

$$+ k_B T \frac{1 + \pi/2}{12} \sigma R_w^2$$

$$\bar{\kappa}_R = \bar{\kappa}_0 \quad (2.20)$$

$$+ \bar{\alpha} \frac{k_B T}{4\pi} \ln(\Psi)$$

$$- k_B T \frac{1}{6} \sigma R_w^2$$

As introduced earlier $\alpha = 3$ and $\bar{\alpha} = -10/3$. Adding the asymmetric sticker polymer to the microemulsion will strongly influence the spontaneous curvature c_0 . The effect

will not be canceled out as is the case for diblock copolymers (2.18). Adding a sticker polymer will therefore increase c_0 as follows:

$$c_{0,eff} = c_0(T) + \frac{1}{4} \sqrt{\frac{\pi}{6}} \frac{k_B T}{\kappa_R} \sigma R_w \quad (2.21)$$

When investigating polymers with a hydrophilic sticker and hydrophobic polymer chain the sign in eq. (2.21) has to be changed since the spontaneous curvature decreases with the addition of the polymer.

Chapter 3

Phase diagram studies

Microemulsions are characterized using a phase diagram which depends on three parameters: the composition of the three substances water, oil and nonionic surfactant (two parameters: α and γ , see (2.2) and (2.3)) and the temperature. A way to display these three-dimensional phase prisms is to use the Gibbs triangle as a base for a perpendicular temperature axis (Figure 3.1). Every point in this prism represents a different composition of the three ingredients water (A), oil (B) and nonionic surfactant (C) at a certain temperature. The water-oil system ($\gamma = 0$) is immiscible for all accessible temperatures.

When investigating the phase behavior of such a system, the volume ratio of water to oil Φ (see (2.4)) is usually fixed. At equal volumes of water and oil ($\Phi = 0.5$) only the amount of surfactant and the temperature are changed. This corresponds to a cut through the three-dimensional phase prism and is called the fish cut due to the characteristic shape of the phase boundaries. This $T(\gamma)$ cut shows all essential points of the system.

3.1 The $T(\gamma)$ phase diagram

Figure 3.2 shows the typical profile of a *fish-like* phase diagram. Four different regions can be distinguished in the phase diagram. For lower surfactant amounts than the CMC-concentration γ_0 (see chapter 2.1) the molecules will be dissolved as monomers (approximately 90% in the oil phase and 10% in the water phase) and have no effect on the phase behavior of the system. In this state the lighter oil will float on top of the water. Increasing the surfactant above γ_0 will lead to three different phase regions depending on the temperature. For low temperatures two phases can be detected. The available surfactant is located inside the lower water phase covering small oil droplets. This region is marked 2, with the bar indicating the position of the surfactant-rich phase. Increasing the temperature will yield three phases, indicated by a 3 in the phase diagram.

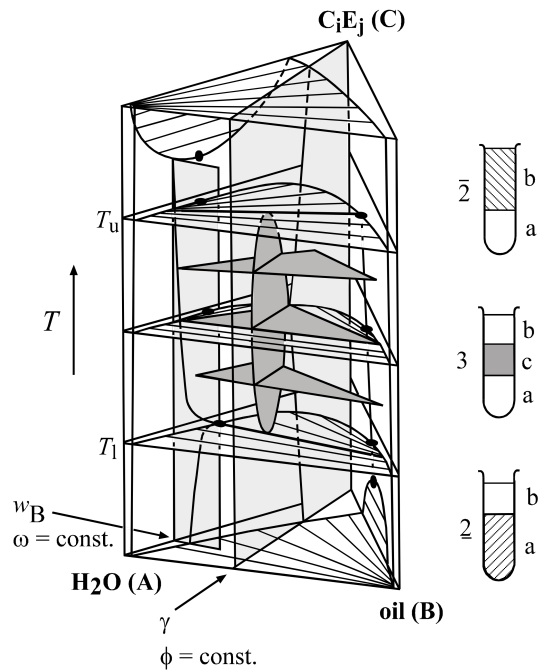


Figure 3.1: Phase prism: A Gibbs triangle with the composition of the system provides a basis for a perpendicular temperature axis. Throughout this work we study symmetric microemulsions with $\Phi = 0.5$ where γ is varied. The other indicated cut aims at droplet microemulsions ($\omega = \text{const.}$, w_B varied) and is not discussed any further.

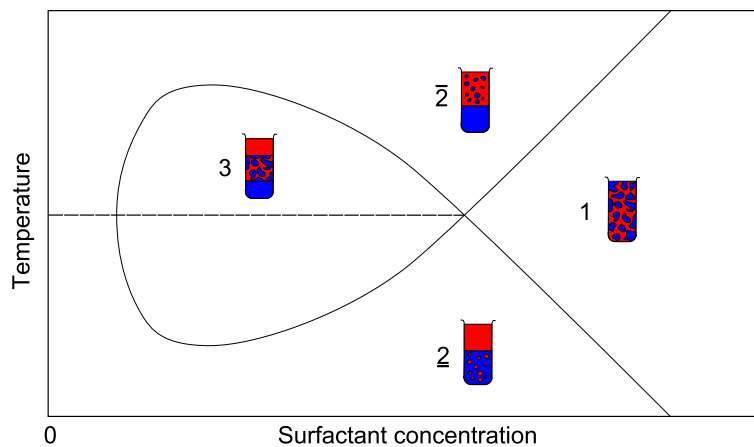


Figure 3.2: Schematic structure of a $T(\gamma)$ fish phase diagram

The microemulsion in the middle is enclosed by an oil (upper) and a water excess (lower) phase. It contains all available surfactant and forms a bicontinuous sponge-like phase on the microscopic length scale. Further increasing the temperature will eventually lead to another two-phase region ($\bar{2}$) where the water excess phase is covered by a water-in-oil microemulsion. The temperature \tilde{T} is called the phase-inversion temperature. Adding surfactant at this temperature will increase the size of the microemulsion until the whole sample is emulsified and the one phase-region (1) is reached. The corresponding point in the phase diagram is called the fish-tail point $X(\tilde{T}, \tilde{\gamma})$, which describes the efficiency of a system: the minimum concentration of surfactant needed to solubilise the entire amount of water and oil. Adding more surfactant will eventually put the system into a lamellar phase, which is of no interest in this work.

The response of the system to temperature changes corresponds to the dependence of microscopic local curvatures on the temperature (Figure 2.3). At low temperatures both curvatures are by definition positive and hence curved towards the oil. Small oil droplets are created within the water. Once one of the curvatures turns negative the sponge phase is reached and the microemulsion is formed between water and oil excess phases. In case both local curvatures are negative, the membrane will curve towards water. As a result of this, small water droplets form in the oil phase.

3.1.1 Analysis of the phase diagrams

As discussed earlier, the position of the fish-tail point $X(\tilde{T}, \tilde{\gamma})$ contains important information about the system. Both the saddle-splay modulus $\bar{\kappa}$ and the spontaneous curvature c_0 can indirectly be measured using its position.

Extracting $\bar{\kappa}$

To extract information about $\bar{\kappa}$ we use (2.20) together with the finding that $\bar{\kappa}_R = 0$ at the fish-tail point [7] and get:

$$\ln(\Psi) = -\frac{4\pi}{\bar{\alpha}} \frac{\bar{\kappa}_0}{k_B T} - \hat{\Xi} \sigma R_w^2 \quad (3.1)$$

When polymers are added to the system, the increase of σR_w^2 is compensated by a decrease of Ψ . Since we know σR_w^2 and measure $\tilde{\gamma}$ at the fish-tail point (which we can use to calculate Ψ) we can make a linear fit to evaluate the parameter $\hat{\Xi}$ and extract $\bar{\kappa}_0$. Theoretically, $\hat{\Xi}$ is predicted to be $-1/6 \cdot 4\pi/\bar{\alpha} = 0.628$.

Extracting c_0

If the mean curvature H is changed by an asymmetric polymer with $R_w \neq R_o$, a change of the phase inversion temperature \tilde{T} is expected since Strey proposed (see chapter 2.2.3):

$$H = \mu_H(T_0 - T) \quad (3.2)$$

For C₁₀E₄ the constant was found to be $\mu_H = 1.42 \cdot 10^{-3} \cdot (\text{K } \text{\AA})^{-1}$ [12].

At the fish-tail point the effective spontaneous curvature is always $c_{0,eff} = 0$ because the membrane does not favor to bend towards oil or water domains. In eq. (2.21) we see that a change of the scaled polymer amount σR_w has to be compensated by a change of the phase inversion temperature \tilde{T} . For sticker polymers we get:

$$c_0(T) = \mu_H(T_0 - T) = \mp \frac{1}{4} \sqrt{\frac{\pi k_B T}{6 \kappa_{eff}}} \sigma R_w \quad (3.3)$$

T_0 is the phase-inversion temperature of the C₁₀E₄ system without polymers. Equation 3.3 allows us to calculate the change of the spontaneous curvature depending on the scaled polymer amount (σR_w).

3.2 Experimental determination of phase diagrams

The phase behavior of microemulsion has been studied in tempered water baths (Figure 3.3). The sample is prepared by filling the test tubes with polymer, surfactant, decane and water. This system is characterized by the mass ratios γ (2.12) and δ (2.11). This test tube is then put into the bath and the temperature is adjusted. After stirring the sample we wait some time until the different phases appear. At low temperatures two phases with a meniscus will quickly form (2). The position of the meniscus moves up with increased temperature until it disappears and the one-phase region is reached (or the three-phase region depending on the surfactant concentration γ). The temperature is then further increased until a new meniscus appears at the bottom of the sample: the upper two-phase region $\bar{2}$ is reached. In this way the temperatures of the phase transitions have been determined. Instead of preparing a new sample with a lower γ value, equal amounts of water and oil are added to the existing system. This decreases γ but changes neither α (we add equal volumes of water and oil) nor δ (since the ratio of

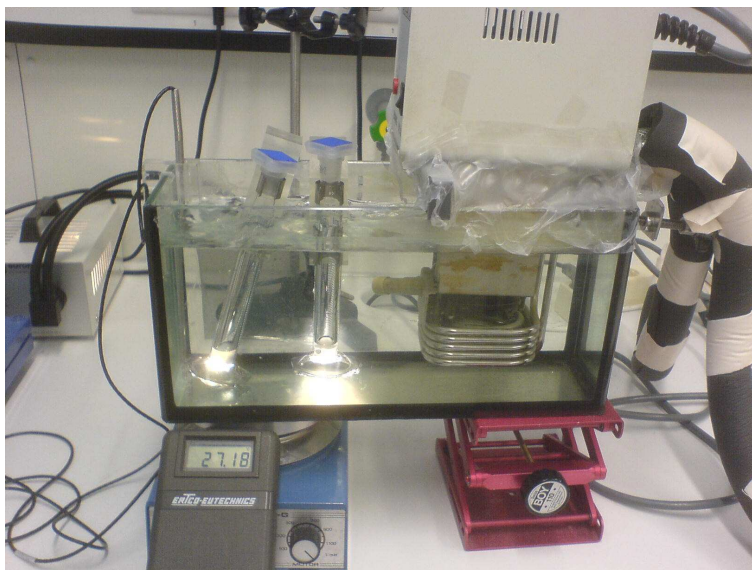


Figure 3.3: Experimental setup for the measurement of the phase diagram. The temperature can be changed in steps of 0.1°C and is measured with the thermometer. After a temperature change the investigated system is stirred and then left untouched. After some time ranging from seconds to hours turbidity indicates phase separation.

polymer to surfactant is not changed). The new system is then once more investigated in the heat bath as described above.

3.3 Interpretation

Plotting the results yields the phase of the system depending on the surfactant concentration γ and the temperature. The boundaries are shown as a solid line (Figure 3.4). The efficiency of a system is extracted from the fish-tail point $X(\tilde{T}, \tilde{\gamma})$, which describes the minimum amount of surfactant needed to emulsify all available water and oil. Phase diagrams for different concentrations of the polymer were investigated in order to quantify the effect of the sticker polymers. Therefore δ was varied from 0% to 10%. A further increase of δ will result in the formation of a lammelar phase instead of a one-phase region. For each of the investigated concentrations of polymer a phase diagram was measured and the fish-tail point was determined and plotted in a γ vs. T graph. It was usually sufficient to measure at surfactant concentrations above $\tilde{\gamma}$ since it is easier to identify the one phase region than to wait for a stabilization of three phases. The fish-tail point was then extrapolated from the existing phase boundaries. By com-

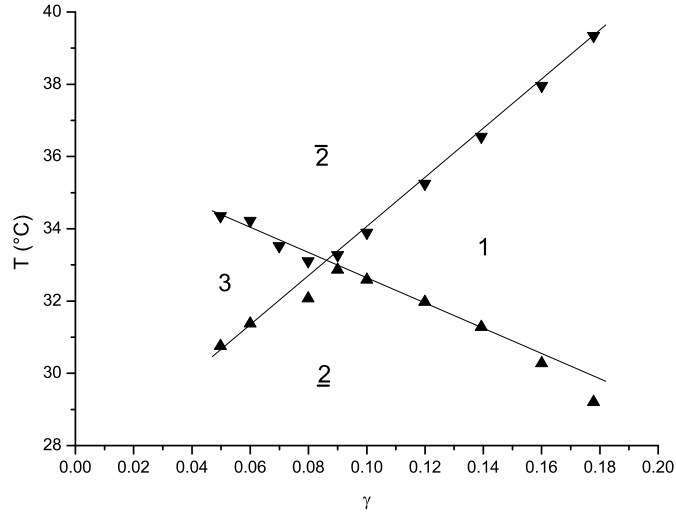


Figure 3.4: Measurement of a phase diagram. In addition to water and oil the surfactant $C_{10}E_4$ was used with the bifunctional sticker polymer $C_{12}(E_{92})_2$ at $\delta = 10\%$.

paring the fish-tail point of different polymer concentrations we were able to extract the efficiency from the decrease of $\tilde{\gamma}$ (see chapter 3.1.1). The spontaneous curvature c_0 was indirectly measured by a change of the temperature \tilde{T} .

For a more general interpretation of the results the mass ratio γ is converted into the membrane volume fraction Ψ . For this we have to keep in mind that the surfactant $C_{10}E_4$ has a solubility of 2wt% in decane and 0.2wt% in water at 30.1°C [13].

$$\Psi = \frac{m_{surfactant} - 0.02 \cdot m_{oil}}{0.959 \left(\frac{m_{D_2O}}{1.105} + \frac{m_{oil}}{0.729} + \frac{m_{surfactant}}{0.974} + \frac{m_{polymer}}{1.035} \right)} \quad (3.4)$$

Chapter 4

Small angle neutron scattering

4.1 General aspects

Small angle neutron scattering (SANS) allows a detailed study of the microscopic structure of microemulsions. In order to describe the scattering process we have to treat the neutron beam as a matter wave to account for interference effects. The wavelength is connected with the momentum by the de Broglie relation: $\lambda = h/p = h/\sqrt{2mE}$. The wave vector is given by $\vec{p} = \hbar\vec{k}$. For now we assume an ideally monochromated beam which hits the sample and is scattered. The change of the wave vector \vec{k} of the neutrons defines the scattering vector \vec{Q} :

$$\vec{Q} = \vec{k} - \vec{k}' \quad (4.1)$$

In the case of elastic scattering, the energy of scattered neutrons is not changed and we get $k = |\vec{k}| = |\vec{k}'| = k'$. We further assume the *Fraunhofer approximation*, where the size of the sample and especially the investigated structure is much smaller than the distance from the source to the sample and from the sample to the detector. The scattering vector is then connected with the scattering angle θ as follows:

$$Q = |\vec{Q}| = \frac{4\pi}{\lambda} \sin \frac{\theta}{2} \quad (4.2)$$

The quantity measured by elastic neutron scattering is the intensity depending on the scattering angle. It is proportional to the differential cross section, which is a measure of the number of neutrons n that are scattered into the solid angle $\Delta\Omega$ normalized to the current of incident neutron flux j :

$$I \sim \frac{d\Sigma}{d\Omega} = \frac{n}{j\Delta\Omega} \quad (4.3)$$

Analysis of the cross section $d\Sigma/d\Omega$ leads to conclusions about the inner structure of the sample. In the so-called *Born approximation* multiple scattering events and refraction (taking place when entering and leaving the sample) are neglected. The total scattering amplitude of a sample can then be evaluated by a superposition of scattering events from all positions within the sample:

$$A(Q) \sim \int_V d^3\vec{r} \rho_s(\vec{r}) e^{i\vec{Q}\vec{r}} \quad (4.4)$$

$\rho_s(\vec{r})$ describes the scattered amplitude at the position \vec{r} within the sample. It is called the scattering length density. Therefore the amplitude A of scattered neutrons is connected with ρ_s by a simple Fourier transformation. Since the intensity $I \sim |A|^2$, the phase information is lost and a simple reconstruction of ρ_s by a Fourier transformation is not possible. However, information about regular arrangements in the sample can be obtained.

The phase difference between two points at the distance l within the sample is $Q \cdot l$. To obtain information on this scale a phase difference of $Q \cdot l \approx 2\pi$ has to be achieved. Using eq. (4.2) we get

$$l \approx \frac{\lambda}{2 \sin(\theta/2)} \approx \frac{\lambda}{\theta} \quad (4.5)$$

We want to measure the regular arrangement of oil and water domains in mircoemulsions. The size of these domains can be as large as several hundred nanometers. As we see in eq. (4.5), measuring structures at this length scale requires either neutrons with similar wavelengths or measurements at small scattering angles θ . Working with wavelengths in the range of 10^2nm (ultra-cold neutrons) creates additional problems. This is why we use small angle neutron scattering together with cold neutrons ($\lambda \sim 4.8\text{\AA}$) in our experiments.

The incoming neutrons only interact with the nuclei of the sample. The scattering cross section of the elements is the relevant parameter for the amplitude of the outgoing wave. The difference of the scattering cross section between hydrogen and deuterium is probably the most important one. Contrast variation methods with these two elements allow a systematic structural investigation of the different parts of a system by

simple substitution. Since we are interested in the oil and water domain structure of microemulsions, the bulk contrast is chosen (use of D_2O instead of H_2O). In general, it is also possible to match the scattering length of water and oil to achieve film contrast. When the scattering length of water, oil and surfactant are matched, it is even possible to perform SANS experiments under polymer contrast [2].

4.2 Experimental details

4.2.1 Setup

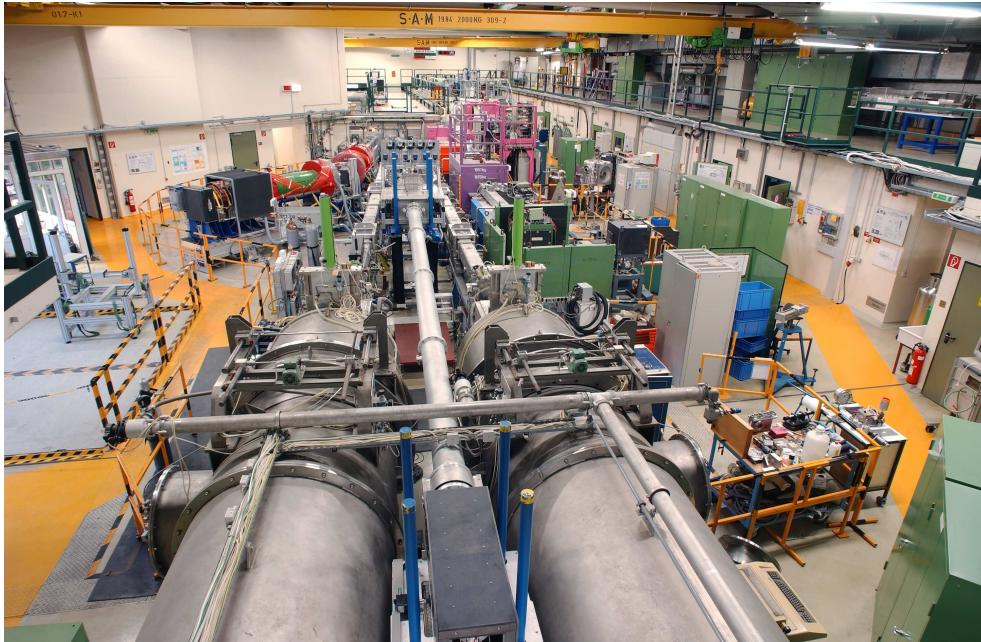


Figure 4.1: KWS2 (left) and the KWS1 (right) at the *Forschungszentrum Jülich*. The detector tube can be seen at the bottom, the collimation at at top of the picture.

All SANS measurements were conducted using the *Kleinwinkelstreuanlage 2* (KWS2) at the *Forschungszentrum Jülich*. The FRJ-2 reactor served as a source for the cold neutrons ($\sim 30K$). After extraction, they are monochromated by a velocity selector, a rotating turbine with neutron absorbing lamellae. In our case the wavelength of the neutrons was set to 6.3\AA with a distribution of $\Delta\lambda/\lambda = 0.1$. The monochromated beam is directed to the collimation aperture by neutron guides. After passing the sample aperture, which defines the divergence of the beam together with the collimation aperture,

Monochromator	Velocity Selector (DORNIER)
λ	6.3 Å (4.8...19 Å)
$\Delta\lambda/\lambda$	0.1
Collimation aperture	$3 \times 3 \text{ cm}^2$ (0.1...3.0 cm)
Collimation length	20 m (1..20 m)
Sample aperture, d_s	$0.8 \times 0.8 \text{ cm}^2$ (0.1..1.4 cm)
Detector distance	1.25...20.0 m
Detector beam stop	$7 \times 7 \text{ cm}^2$
Detector area	$50 \times 50 \text{ cm}^2$
Q -range	$2 \cdot 10^{-3} - 0.2 \text{ \AA}^{-1}$
Neutron flux at sample	$10^5 - 6 \cdot 10^6 \text{ n}/(\text{cm}^2\text{s})$

Table 4.1: Instrument details of the KWS2 at the Forschungszentrum Jülich

the neutrons hit the sample and are partially scattered. These scattered neutrons hit the detector, whereas unscattered neutrons will hit the beamstop, which shields the detector from the high intensity of the direct neutron beam. The distance between the detector and the sample can be varied from 1.25 to 20 meters by moving the whole detector through a vacuum tube. This enables us to cover different scattering vectors Q . High detector distances correspond to small Q vectors. The collimation distance can also be changed from 1 to 20 meters in order to vary the resolution and the flux of the beam. Details about the instrument can be found in table 4.1.

The detection technique bases on a Li-scintillation glass with photo multipliers. A high efficiency of $\sim 99\%$ can be reached for scintillation detectors. The two-dimensional detector has an active area of $50 \times 50 \text{ cm}^2$ with a spatial resolution of $0.525 \times 0.525 \text{ cm}^2$ for one detector pixel. For cold neutrons the reaction $n+{}^6\text{Li}$ has a large cross-section (941 barn for 25meV neutrons [14]). The detector features a low dead time of only $4\mu\text{s}$ with a maximum count rate of 25kHz.

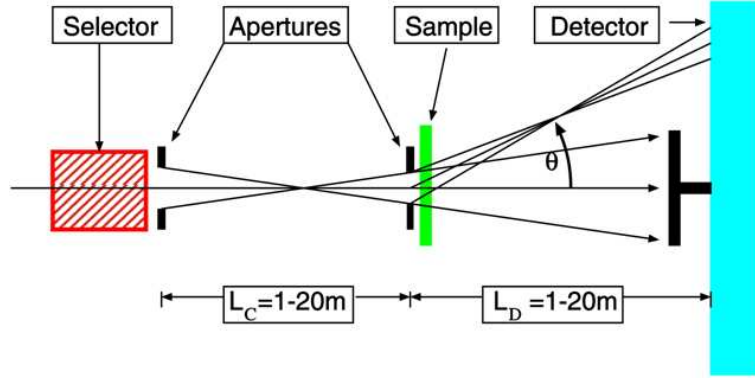


Figure 4.2: Neutrons from the detector are monochromated in the selector and focused by the apertures. After being scattered at the sample the neutrons are detected. Non-scattered neutrons hit the beam-stop.

4.2.2 Corrections

Absolute calibration

The measured intensity of neutrons at the detector has to be corrected for errors induced by the experimental setup. The differential cross section and the intensity are connected by

$$I = I_i D_e \Delta\Omega A T d \frac{d\Sigma}{d\Omega} \quad (4.6)$$

I_i represents the incident beam intensity, D_e is the detector efficiency, $\Delta\Omega$ the angle of a single detector element, A the sample area, d the sample thickness and T the transmission of the sample. The intensity I depends on the specific instrument used for the measurements. Opposed to that the differential cross section $d\Sigma/d\Omega$ is specific for the investigated sample and independent of the experimental setup.

To obtain a sample specific information all measurements are normalized to a reference material (plexiglass in our case). Using the indices s for the sample and pl for plexiglass we compare the measurement with the reference material:

$$\left(\frac{d\Sigma}{d\Omega}\right)_s = \frac{I_s}{I_{pl}} \frac{L_s^2}{L_{pl}^2} \frac{d_{pl}}{d_s} \frac{T_{pl}}{T_s} \left(\frac{d\Sigma}{d\Omega}\right)_{pl} \quad (4.7)$$

We define the calibration constant as $\mu_{pl} = d_{pl} T_{pl} \left(\frac{d\Sigma}{d\Omega}\right)_{pl}$. For a neutron beam with

$\lambda = 6.3\text{\AA}$ we use $\mu_{pl}(6.3\text{\AA}) = 0.052$. The measurements of the sample and the plexiglass can be performed at different detector distances. A smaller L_{pl} leads to better statistics while L_s is adjusted to the desired Q-range.

With $C = I_{pl}T_s d_s L_{pl}^2 / L_s^2$ we can write the scattering cross-section as:

$$\left(\frac{d\Sigma}{d\Omega}\right)_s = \frac{\mu}{C} I_s \quad (4.8)$$

The error caused by scattering of the sample container is corrected by measuring the intensity of an empty cell and subtracting it from the sample measurement. With this final correction we receive:

$$\left(\frac{d\Sigma}{d\Omega}\right)_s = \frac{\mu}{C} \frac{I_s - I_{ec}(T_s/T_{ec})}{I_{pl} - I_{ec}(T_{pl}/T_{ec})} \quad (4.9)$$

With eq. (4.2) we then get the scattering cross-section as function of the scattering vector $d\Sigma/d\Omega(Q)$.

Radial averaging

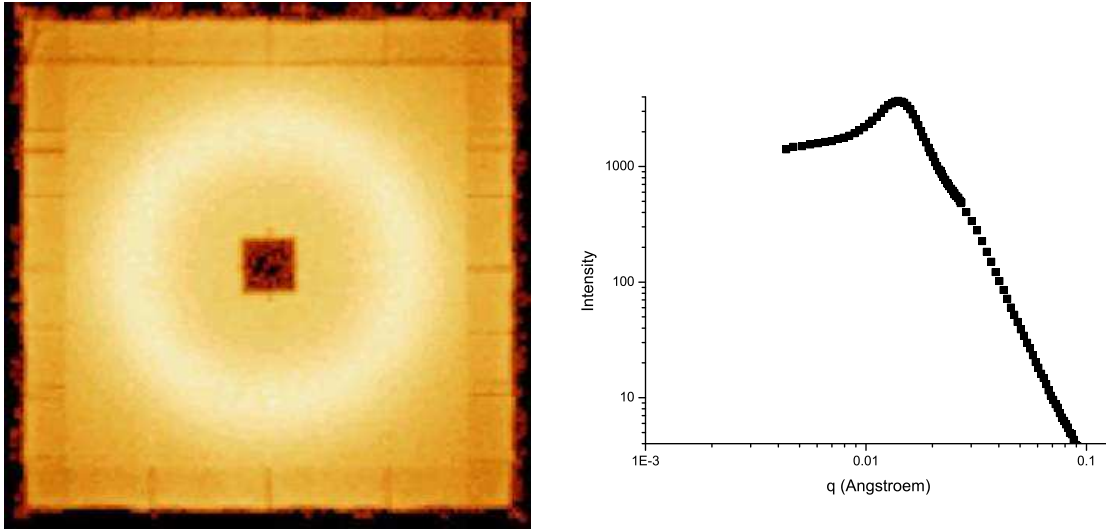


Figure 4.3: Left: typical detector image with logarithmic color scale. The square in the middle is caused by the beamstop. Right: corresponding scattering function $I(Q)$ plotted logarithmically.

After absolute calibration, the two-dimensional detector image has to be converted into the scattering function $(d\Sigma/d\Omega)(Q)$. Since the investigated microemulsions are isotropic, the detector image shows a spherically symmetric distribution of the scattered neutrons. We now determine the center of this distribution ($Q = 0$) and integrate the intensities for the different Q -vectors. After a radial normalization we obtain the scattering function as a function of the scattering vector Q (Figure 4.3).

Resolution correction

The limited resolution of the neutron detector causes a smearing of the measured scattering intensity. To describe this effect mathematically the real scattering function is convolved with a distribution (resolution) function $R(Q, Q_0)$ [15]:

$$I(Q) = \int dQ R(Q, Q_0) \frac{d\Sigma}{\Delta\Omega} \quad (4.10)$$

The distribution function for radially averaged data is given as:

$$R(Q, Q_0) = \frac{Q}{\sigma_{Q_0}^2} \exp \left[-\frac{Q^2 + Q_0^2}{2\sigma_{Q_0}^2} \right] I_0 \left[\frac{QQ_0}{\sigma_{Q_0}^2} \right] \quad (4.11)$$

$\sigma_{Q_0}^2$ describes the smearing effects caused by the wavelength spread, finite collimation and the detector resolution. I_0 is a modified Bessel function that accounts for the radial averaging. This resolution distribution function is taken into consideration when fitting the Teubner-Strey formula to the calibrated scattering cross section.

4.3 Scattering on microemulsions

4.3.1 The Gaussian Random Field approximation

The Gaussian Random Field (GRF) approximation models a microemulsion with a scalar field $h(\vec{r}) = \alpha$ where $-\infty < \alpha < \infty$. Oil and water domains are represented respectively by negative and positive values of α . The interface at the phase inversion temperature \tilde{T} is found at positions \vec{r} where $h(\vec{r}) = 0$. For a temperature $T > \tilde{T}$ the membrane is found at higher cutting values of α . This corresponds to a curvature towards water domains. $h(\vec{r})$ has to meet additional normalization requirements: $\langle h^2(\vec{r}) \rangle = 1$. For equal volumes of water and oil $\langle h(\vec{r}) \rangle = 0$.

The statistic of this scalar field is defined by the quadratic Hamiltonian

$$\mathcal{H}_0 = \frac{1}{2} \int d\vec{r} h(\vec{r}) w(\vec{r} - \vec{r}') h(\vec{r}') \quad (4.12)$$

where $w(\vec{r} - \vec{r}')$ is the coupling function. Thermal fluctuations of the scalar field $h(\vec{r})$ are calculated using the Boltzmann weight $e^{-\mathcal{H}_0}$. Using the GRF model, we can now analytically calculate the average geometry of the surface after defining the coupling function $w(\vec{r} - \vec{r}')$. w is expected to decay rapidly with $(\vec{r} - \vec{r}')$ in order to make the integral and the second and fourth moments finite.

Pieruschka and Safran have implemented a variational approach method to describe the coupling function $w(\vec{r} - \vec{r}')$ or $w(\vec{q})$ [16]. This approach leads to the Teubner-Strey formula:

$$G(q) = \frac{1}{w(q)} = \frac{a}{q^4 - bq^2 + c} \quad (4.13)$$

a , b and c are parameters depending on the bending rigidity κ and the surface to volume fraction $S/V = \Psi/a$. The correlation function can be obtained by a Fourier transformation of (4.13), which is analytically possible due its simple form:

$$G(\nu) = \int \frac{d^3q}{(2\pi)^3} G(q) e^{-i\vec{q}\vec{r}} = \frac{1}{k_0 r} e^{-r/\xi} \sin(k_0 r) \quad (4.14)$$

with $\xi = 2/\sqrt{2\sqrt{c} + b}$. k_0 is the characteristic wave vector and is connected with

(4.13) by $k_0 = \frac{1}{2}\sqrt{2\sqrt{c}-b}$. k_0 is connected to the domain size by $k_0 = d/2\pi$. This relation gives us the possibility to calculate the microscopic parameters d and ξ with the experimentally obtained scattering function. The bending rigidity κ can be received from k_0 and ξ for sufficiently large κ by [2]:

$$k_0\xi = \frac{64}{5\sqrt{3}} \frac{\kappa}{k_B T} \quad (4.15)$$

4.3.2 The Ginzburg-Landau model

Teubner and Strey have calculated the scattering function for the bulk contrast on the basis of the Ginzburg-Landau model [4]. In this approach the Landau free energy is approximated by an order parameter which is chosen to be larger than the microscopic length scales and at the same time small compared to the macroscopic length scales of the system. For microemulsions this order parameter, Ψ , is connected to the water-to-oil ratio. The simplest approximation for the free energy function is:

$$F(\Psi) = \int d\vec{r} (a_0\Psi^2 + a_1(\vec{\nabla}\Psi)^2 + a_2(\Delta\Psi)^2) \quad (4.16)$$

With this functional the scattering intensity distribution is found to be:

$$\frac{d\sigma}{d\Omega}(Q) \sim \frac{1}{a_0 + a_1Q^2 + a_2Q^4} \quad (4.17)$$

For large Q values this function decays with Q^{-4} . Thus we get the two-point correlation function for spherical symmetry:

$$\langle \Psi(\vec{r}_1)\Psi(\vec{r}_2) \rangle = \int d\vec{Q} e^{-i\vec{Q}(\vec{r}_2-\vec{r}_1)} S(\vec{Q}) = G(|\vec{r}_2 - \vec{r}_1|) \quad (4.18)$$

The correlation function is then:

$$G(r) = 4\pi \int_0^\infty dQ Q^2 \frac{\sin(Qr)}{Qr} S(Q) \quad (4.19)$$

which leads to

$$G(r) = \frac{1}{k_0 r} e^{-r/\xi} \sin(k_0 r) \quad (4.20)$$

with the correlation length ξ and $k_0 = 2\pi/d$. After determining the proportionality constant in (4.17) we obtain the Teubner-Strey formula:

$$\frac{d\Sigma}{d\Omega}(Q) = \frac{8\pi \langle \nu^2 \rangle / \xi}{Q^4 - 2(k_0^2 - \xi^{-2})Q^2 + (k_0^2 + \xi^{-2})^4} \quad (4.21)$$

$\langle \nu^2 \rangle \equiv \langle (\rho - \bar{\rho})^2 \rangle$ is the mean square scattering length density fluctuation, which can be approximated by $\langle \nu^2 \rangle = \Phi_o \Phi_w \Delta\rho^2$. Φ_o and Φ_w are the volume fractions of oil and water, $\Delta\rho$ is the difference of the scattering length densities of oil and water.

Chapter 5

Materials

Five different sticker polymers have been investigated. Three of these polymers consist of one or two long hydrophilic chains and a short hydrophobic part. Their structure is the same as that of the used surfactant, $C_{10}E_4$, only with a longer ethylene oxide chain. The polymeric chain consists of about 90 ethylene oxide (CH_2-CH_2-O) molecules. Ethylene oxide is a polar molecule due to the electronegativity of the oxygen atom and hence responsible for the hydrophilic behavior of this part of the polymer. The chain is then continued by several carbon atoms (CH_2). This short piece, the sticker, is hydrophobic and supposed to anchor in the oil domains of the microemulsion. Contrary to these polymers, the other two have an ionic sticker (hydrophilic) and a long hydrophobic chain. A schematic drawing of these polymers at the water-oil interface can be seen in Figure 5.1. A list of the investigated polymers can be found in Table 5.1.

5.1 Synthesis and characterization of the anionic sticker polymers

The three polymers with hydrophobic sticker ($C_{12}E_{90}$, $C_{12}(E_{92})_2$ and $C_{16}(E_{87})_2$) have been synthesized at the Forschungszentrum Jülich. For the monofunctional sticker polymers the synthesis is started with alcohol $CH_3-(CH_2)_n-CH_2-OH$, which is activated by a potassium based initiator. The amount of potassium is chosen to replace approximately 20% of the OH groups of the alcohol and form $CH_3-(CH_2)_n-CH_2-OK$. The single potassium atom is in constant exchange with OH groups of the other alcohols. This new mixture of alcohols is now merged with ethylene oxide monomers ($-CH_2-CH_2-O$ -rings) inside a chemical reactor. The aggressive $-OK$ group is able to open an ethylene oxide ring and appends it into the chain. We are left with a longer activated chain. The process of opening an ethylene oxide ring occurs on much larger timescales than the frequent exchange of potassium atoms. This way all available alcohol groups grow at a

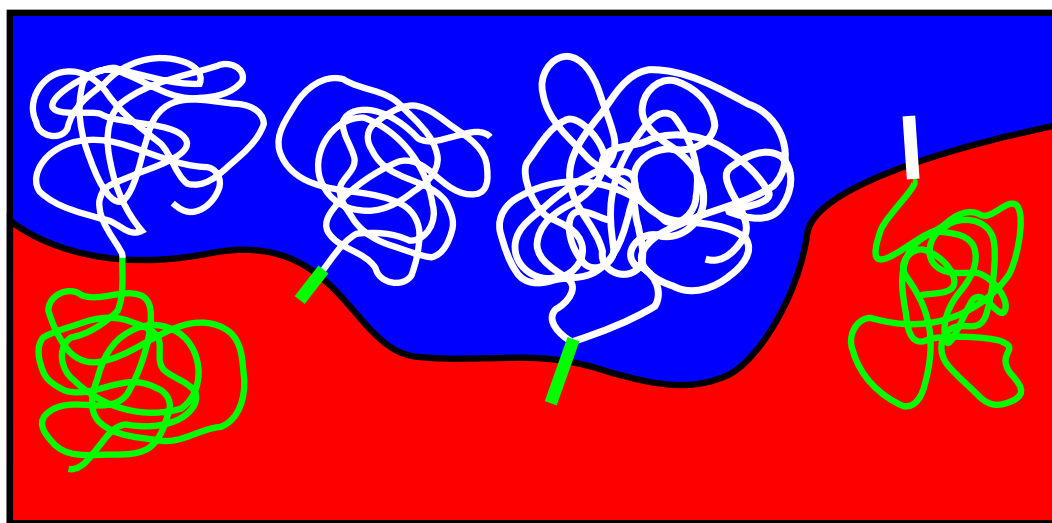


Figure 5.1: Diblock copolymer (left) and three different sticker polymers active at the water (blue) and oil (red) interface. The short sticker will anchor the polymer in the membrane and the hydrophilic chain will form a mushroom-like shape due to entropic reasons. The bifunctional sticker has two polymeric arms, and the ionic sticker has a long hydrophobic polymeric area.

Polymer	Description
$C_{12}E_{90}$	Sticker polymer with one arm
$C_{12}(E_{92})_2$	Sticker polymer with two hydrophilic arms
$C_{16}(E_{87})_2$	Sticker polymer with two hydrophilic arms and a longer sticker
$(CH_2=CHCOOC_4H_9)_{54}-COOH$	Ionic sticker polymer containing of 54 (t-butyl acrylate) monomers and a carboxyl group as ionic sticker
$(CH_2-CH=CH-CH_2)_{192}-COOH$	Ionic sticker polymer with polybutadiene as hydrophobic chain and a carboxyl group as ionic sticker

Table 5.1: List of investigated polymers

constant speed and in equal lengths. After using up all available ethylene oxide acetic acid is added to the system to deactivate the potassium atoms and replace them with hydrogen. The potassium salt is removed by washing the polymer in chloroform and water mixtures. For the synthesis of the bifunctional sticker polymers different alcohols with two OH groups are chosen as the base material. The rest of the process stays unchanged and two ethylene oxide chains grow from the initiated molecule.

The initiators of the bifunctional sticker polymers are 1,2-dodecanol and 1,2-hexadecanol. Thus the ethylene oxide chains grow from different parts of the alkyl chain and leave only 10 and 14 hydrophobic carbon atoms behind.

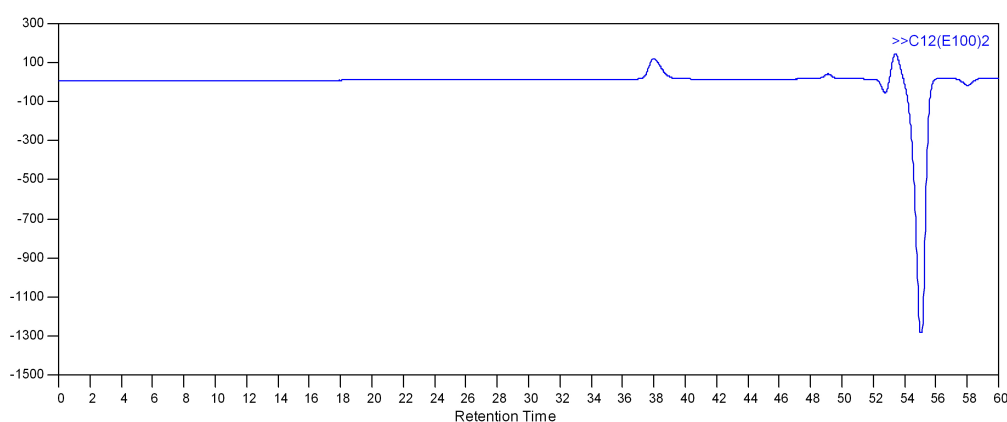


Figure 5.2: GPC-analysis of C₁₂(E₉₂)₂.

For the synthesized sticker polymers the length of the ethylene oxide chains has been determined by gel permeation chromatography (GPC), also called size exclusion chromatography (SEC). The concept of this analysis is that particles (in our case polymers) of different size will flow through a specialized tube at different rates. This tube contains extremely small porous polymer beads with pores of different sizes. Large polymers will flow through the tube more quickly since they can not enter as many pores as smaller polymers. After filling the tube with the polymer in solution, the intensity of the exiting fluid in dependence of the time is measured. Comparing this curve with a reference measurement (performed with particles of known length) allows the determination of the polymer's volume and therefore the length. The GPC-analysis of C₁₂(E₉₂)₂ can be seen in Figure 5.2. The peak of the polymer is found at a retention time of ~ 38 min. Later signals arise from the solvent.

The hydrophilic chain of all three synthesized polymers was supposed to consist of approximately 100 ethylene oxide monomers. An exact predefinition during the synthesis is not possible which is why the real length is later determined with GPC.

The distribution of these lengths is represented by the width of the peak. This distribution is specified by the polydispersity index (PDI) which is calculated by dividing the weight average molecular weight M_w by the number average molar mass M_n . The PDI approaches 1 as the polymer chain lengths reach a tight distribution. The investigated polymers had a PDI of $M_w/M_n < 1.1$.

5.2 Characterization of the ionic sticker polymers

The end-group of both ionic sticker polymers is formed by a carboxylic acid (COOH). Only the hydrophobic chain is different: for the first of the two, monocarboxy terminated poly(*t*-butyl acrylate), approximately 54 $[\text{CH}_2=\text{CHCOOC}_4\text{H}_9]$ monomers form the hydrophobic part. For the second sticker polymer, monocarboxy terminated polybutadiene, 192 polybutadiene monomers $[\text{CH}_2-\text{CH}=\text{CH}-\text{CH}_2]$ provide the basis for the chain. Both polymers were bought from the Canadian company *Polymer Source*. According to the provided characterization the polymers have a functionality better than 98% and a PDI better than 1.1. Own GPC measurements verified this statement. The carboxyl end-group is a weak acid since it will only partly dissociate into R-COO^- anions and H^+ cations in water. It is therefore necessary to increase the pH value of the water to create a base so that free OH^- -particles are able to join with the H^+ cations of the carboxylic acid. The COO^- group then functions as a sticker and will attach the polymer to the water domains while the hydrophobic chain stays in the oil domains.

COOH-poly(*t*-butyl acrylate) is a rather bulky polymer with a short chain length and relatively large side groups on every monomer of the chain. The second polymer, COOH-polybutadiene, has a much longer chain composed of linear monomers without side group. It is expected to behave more ideally than the first one, which might not form a Gaussian chain.

Chapter 6

Experiments

We will now discuss the experiments performed to measure the thermodynamical parameters κ , $\bar{\kappa}$ and c_0 . Therefore we first look at the measured phase diagrams of the microemulsions and after that describe the small angle neutron scattering experiments.

6.1 Phase diagrams

6.1.1 Nonionic sticker polymers

The earlier discussed boosting effect (chapter 2.3) can be quantified by investigating phase diagram measurements. The macroscopic result, a strong increase of the microemulsion phase coexisting with other phases (Figure 2.4), appears in concert with a change of the position of the fish-tail point in the phase diagram. Figure 6.1 shows the fish diagram for the first of the five investigated sticker polymers C₁₂E₉₀. The fraction of polymer is measured with δ (see eq. (2.11)) and ranges from 0% up to 10%. For the connected points in Figure 6.1 δ is constant. Three samples were prepared for every polymer concentration. The amount of surfactant was chosen such that the first sample was just inside the one-phase region. For the second and third sample the amount of surfactant γ was increased by 1.5% respectively. This approach has three advantages: first of all putting the sample inside the one-phase region ensures an accurate investigation of the phase boundary since it is easier to distinguish between a one- and a two-phase region than it is to differentiate between a two- and a three-phase region which are both turbid. The second reason is that the phase boundary in this region changes almost linearly with the surfactant amount which makes an extrapolation to the fish-tail point easier and more exact. Third it allows for a reuse of the samples for the SANS measurements, which have to be performed in the one-phase region. Therefore we have directly used D_2O instead of water which is only supposed to shift the temperature of the phase

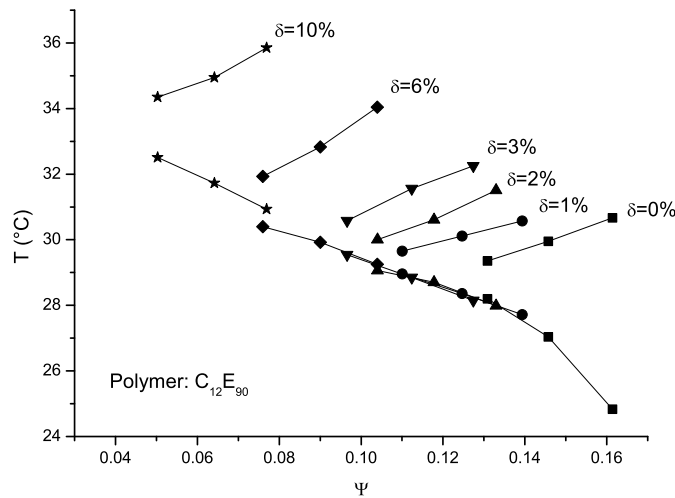


Figure 6.1: The boosting effect visualized with phase diagrams: With increasing polymer amount δ the fish-tail point is shifted to lower surfactant concentrations and different temperatures \tilde{T} .

diagram down by approximately 1°C [17].

When investigating Figure 6.1 one sees that the lower phase boundary stays almost constant with increased polymer amount whereas the upper boundary is shifted to higher temperatures. This fact is connected to the polymer which acts only in the water-phase. The result is a shift of the fish-tail point to lower surfactant concentrations and an increase of the phase inversion temperature \tilde{T} .

Comparing these measurements with the bifunctional sticker polymer $C_{12}(E_{92})_2$ (see Figure 6.2) reveals the intensity of the boosting effect. It is clearly observable that the same weight amount of polymer influences the phase diagram only about half as much as the monofunctional sticker did. This weak dependence raises the question whether all of the added polymers are active at the interface. To get an estimate about this value we decided to prepare a sample in the three phase region with a polymer amount of $\delta = 10\%$. After temperating the system to the phase inversion temperature, two equally sized excess phases started to appear above and below the microemulsion. Since the polymer in question is mainly composed of hydrophilic parts we expect it to be solved in the water excess phase or the water domains inside the microemulsions if not active at the interface. Evaluating the amount of polymer solved in the water excess phase should therefore give a rough estimate about its activity.

The water-excess phase was extracted with a syringe after the system had stabilized.

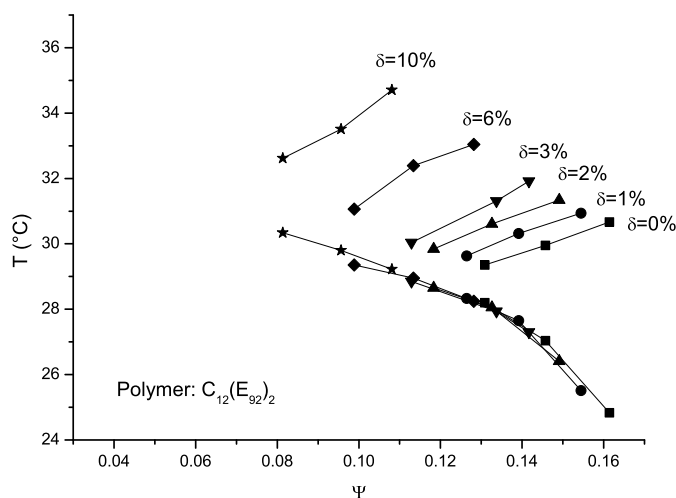


Figure 6.2: Phase diagram measurements for the bifunctional sticker polymer $C_{12}(E_{92})_2$, $C_{10}E_4$, decane and deuterium.

After weighing the sample it was freeze-dried. After three days all water had sublimated and the sample was once again weighed to determine the mass of the remaining material. Further a GPC-analysis was performed to determine the amount of polymer inside the residue. With these values we were able to calculate the amount of polymer located inside the water-excess phase. This whole procedure was repeated for several points inside the three phase region to get a better estimate.

It was found that the amount of inactive polymer ranged from 20% up to 50% depending on the position within the three-phase region. Any polymer solved in the water-excess phase is not able to contribute to a boosting effect of the microemulsion. The sticker consisting of twelve carbon atoms that anchors the polymer in the membrane is not long enough to balance the entropic force of the two hydrophilic chains that try to pull away from the interface. The same test was also conducted for $C_{12}E_{90}$ with the result that a maximum of 1% of the polymer was found in the water-excess phase.

This method does not assert the claim to make an exact assumption about the active polymers, nevertheless it gives an upper limit since any polymer in the water excess phase is not contributing to any effects at the interfaces. The question how much polymer is dissociated in the water domains of the microemulsion, and therefore non-active, remains. This is particularly interesting since the analyzed system of this work were completely emulsified.

In order to prevent the chains from pulling the sticker out of the interface a similar

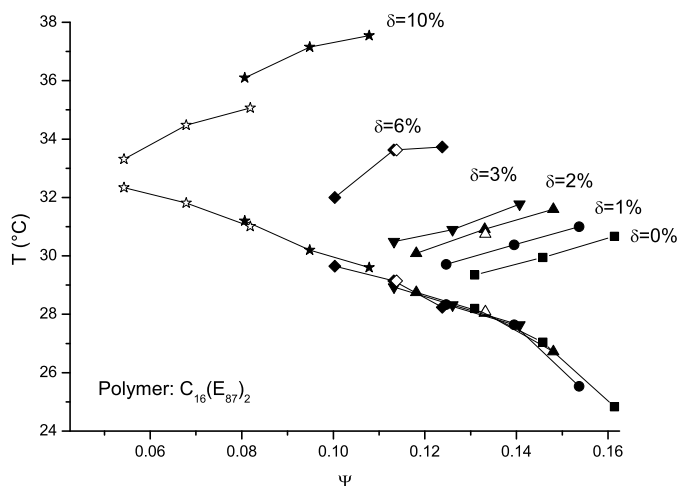


Figure 6.3: Phase diagram for the bifunctional polymer $C_{16}(E_{87})_2$ which has four additional carbon atoms at the sticker to provide a stronger anchor.

polymer with longer sticker was synthesized: $C_{16}(E_{87})_2$. Figure 6.3 shows the phase diagram of this *upgraded* polymer. One immediately sees a strong boosting effect for $\delta = 10\%$, similar to the one of the monofunctional sticker $C_{12}E_{90}$. This implies an improved behavior at the interface. Once again the activity of the polymer at the interface was tested with the method described above and showed similar results as the test with the monofunctional sticker: no more than 2% of the total polymer added to the system were found in the water-excess phase.

6.1.2 Ionic sticker polymers

When investigating monofunctional ionic sticker polymers a further variable has to be regarded: the pH-value of the system. The sticker of the polymer consists of a carboxylic acid (COOH). In order to attach this sticker inside the water domains free OH^- particles have to be available. This is achieved by adding sodium hydroxide (NaOH) to the system. Since we know the molecular weight of the polymers (7000 g/mol) and that of NaOH we are able to specify the allocation of the COOH groups by adding a certain amount of NaOH for a given amount of polymer. We have investigated three different pH-values: 13, 12 and 11.2. For pH 13 and $\delta = 10\%$ every COOH-sticker of the polymers is allocated by about ten OH^- particles. The phase diagrams for this allocation can be seen in Figure 6.4. The first significant difference to the earlier investigated sticker polymers is that the upper phase boundary stays almost constant with the addition of

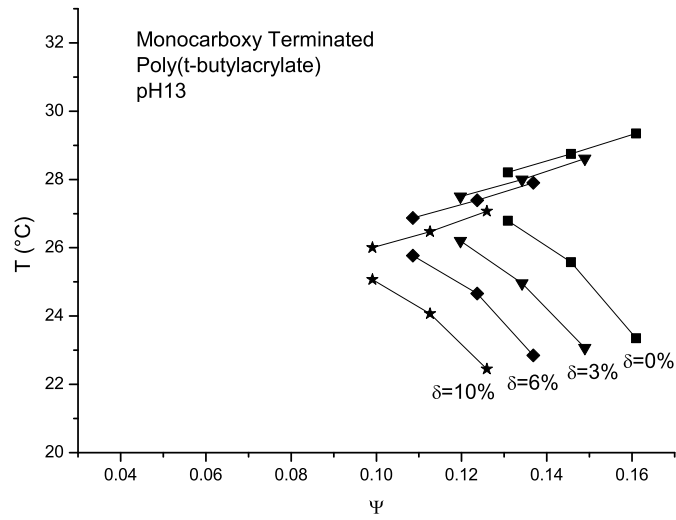


Figure 6.4: Phase diagram for monocarboxy terminated poly(t-butyl acrylate) with a pH-value of 13. At $\delta = 10\%$ about ten OH^- -particles are available for every polymer in the water domains which should ensure that chains are able to anchor at the interface.

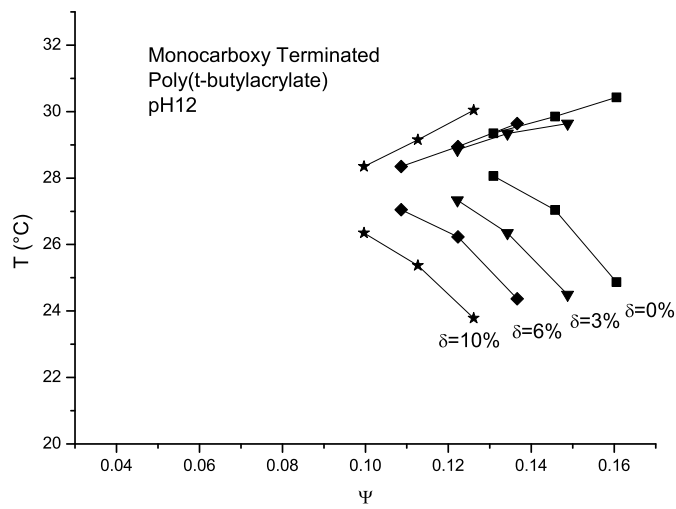


Figure 6.5: Phase diagram for monocarboxy Terminated Poly(t-butyl acrylate) with a pH-value of 12. At this pH-value roughly one OH^- -particle is available per polymer at $\delta = 10\%$

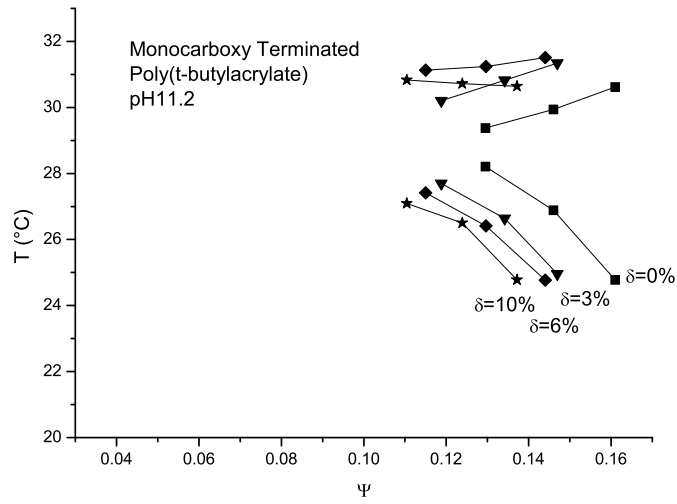


Figure 6.6: Monocarboxy terminated poly(*t*-butylacrylate) with a pH-value of 11.2. The available NaOH is able to allocate the polymer up to $\delta = 3\%$. A further increase of the polymer has only a small effect on the phase diagram.

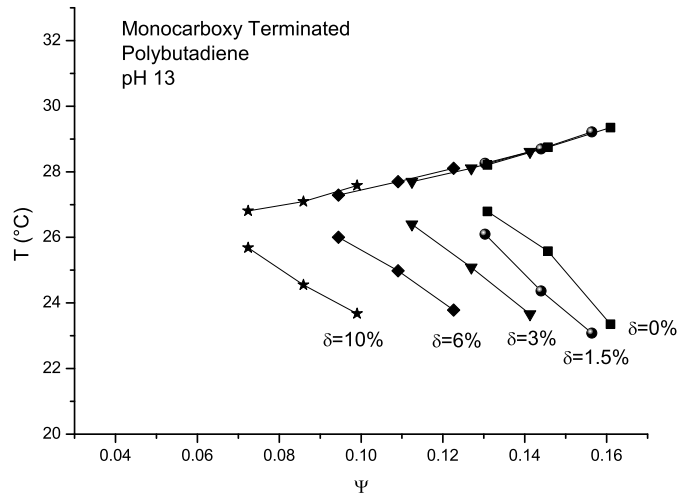


Figure 6.7: Monocarboxy terminated polybutadiene at a pH-value of 13.

polymers because the investigated polymer is active in the oil-phase. This is of course due to the inverse nature of these polymers (compared to $C_{12}E_{90}$) with a hydrophilic sticker and hydrophobic chain. As we expected from eq. (2.18) this causes a decrease of the phase inversion temperature. We also notice that the boosting effect is not as strong as it is for the monofunctional stickers discussed earlier.

Comparing the measurement with no polymer ($\delta = 0\%$) with the ones taken earlier without NaOH (figure 6.1) we see a shift of the phase boundaries to lower temperatures which causes the phase inversion temperature \tilde{T} to decrease. Since the only difference in these systems is the pH value, the addition of NaOH must be the cause for the temperature shift. This effect was explained by Kahlweit and Strey [18, 19]. The addition of lyotropic substances, such as NaOH, causes an increased polarity of water. This increased polarity gives rise to a change of the spontaneous curvature and with that a change of the phase-boundaries to lower temperatures.

The second series was measured at a pH-value of 12 (Figure 6.5). For $\delta = 10\%$ one OH^- -particle is available for each polymer chain. As expected we see a similar boosting effect as above since all available polymers should be able to attach to the interface. Additionally, all phase boundaries are shifted to higher temperatures compared to the one with a pH-value of 13. This is consistent with the earlier discussed effect of NaOH on the spontaneous curvature.

The lowest pH-value investigated (pH 11.2) has just enough OH^- to cover a polymer amount of $\delta = 3\%$. Any additional polymer is not able to attach to the interface since no free OH^- -particles are available in the water domains. This effect is clearly visible in the phase diagram of the system (Figure 6.6). Adding more polymer than $\delta = 3\%$ causes almost no additional boosting of the system. The allocation of the polymer was also visually confirmed by the samples with $\delta > 3\%$. Bunches of unsolved (precipitated) polymer were floating inside the microemulsion which made a differentiation between the one-phase and the two-phase regions difficult. We also note that this small amount of NaOH has no effect on the phase inversion temperature.

We investigated the last polymer, monocarboxy terminated polybutadiene, only for a pH-value of 13 to make that sure that all polymer stickers were able to anchor in the interface and allow us to omit any effects concerning the allocation of the $COOH$ -stickers. The results can be seen in Figure 6.6. Once again we see the expected decrease of the phase inversion temperature with the addition of polymer and also note a stronger boosting effect compared to the first ionic sticker polymer.

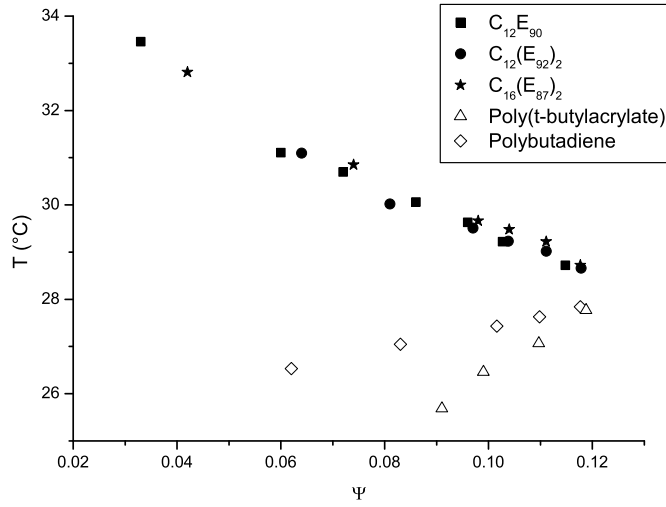


Figure 6.8: Position of the fish-tail point for all investigated polymers. The relative concentration of the polymer δ is (from right to left) 0%, 3%, 6% and 10%.

6.1.3 Investigation of the fish-tail points

With the above discussed phase diagrams we are able to estimate the position of the fish-tail point for each polymer concentration. Figure 6.8 shows the fish-tail points for all investigated sticker polymers at concentrations δ ranging from 0% to 10%. For the first of the two ionic sticker polymers, COOH-poly(t-butyl acrylate), we only show the measurements for pH 13 since we are sure that the polymer is active at the interface for this configuration. One can see the change of the phase inversion temperature for the solutions without polymer (far right) for different pH values. The upper points correspond to the ternary deuterium, decane and C₁₀E₄ system, the lower two points represent the same microemulsion with the addition of sodium hydroxide. As we add the polymer to the system the minimum amount of surfactant to emulsify the whole system $\tilde{\Psi}$ decreases and the phase inversion temperature \tilde{T} changes. \tilde{T} increases for the non-ionic sticker polymers which are active in the water domains and cause a preferred curvature towards oil domains. \tilde{T} decreases for the ionic sticker polymers respectively.

With figure 6.8 we are able to compare the boosting effect depending on the relative weight ratio of the polymer to the surfactant δ . The monofunctional non-ionic sticker polymer C₁₂E₉₀ shows the strongest boosting for $\delta = 10\%$. It is immediately followed by the bifunctional polymer C₁₆(E₈₇)₂. As we have seen earlier, C₁₂(E₉₂)₂ is not fully active at the interface and therefore exhibits a weak boosting effect. The two nonionic sticker polymers both show a lower boosting effect but their different chemical structure

compared to the non-ionic stickers makes a comparison difficult.

6.2 SANS measurements

To measure the domain size d and the correlation length ξ , SANS measurements were performed with the bulk contrast where water of the microemulsions is replaced by heavy water. As seen earlier, all samples are prepared with enough surfactant to be in the one phase region. Three values for γ are investigated for every polymer concentration δ . Since the polymer influences the minimum amount of surfactant necessary to reach the one phase region all samples are measured at different surfactant amounts.

6.2.1 Sample preparation and measurement

Before the measurement the sample was put in a heat bath and tempered to the phase inversion temperature \tilde{T} . It was then filled into quartz cells (1mm sample thickness) which were transferred into a cell container positioned in the neutron beam. We were able to adjust the temperature of this container within 0.1°C. Each sample is irradiated for 10 minutes at two detector distances to cover the full Q -range. The collimation is set to 20m, maximizing the resolution of the neutron beam.

6.2.2 Discussion of scattering functions

After the correction and radial averaging of the measured data (see chapters 4.2.2 and 4.2.2) we receive the scattering cross section in dependence of the scattering vector Q . To understand this information about the microscopic structure of the sample we will now discuss the obtained scattering curves. Figure 6.9 shows three SANS measurements. The lowest curve has the lowest surface to volume fraction Ψ . The curve in the middle was multiplied by 10 to make the comparison easier and has more surfactant (γ increased by 1.5wt%). The last curve has the largest amount of surfactant und was mutliplied by 100. Low scattering vectors Q represent the structure at large scales. Therefore a constant high value of the scattering cross section for low Q values hints at strong fluctuations on large length scales. The peak in the middle at about 0.015\AA^{-1} represents the typical length scale of the microemulsions. The domain size d can be estimated from this charateristic length by $d \approx (2\pi)/Q_{max}$. The correlation length ξ is associated with the width of this peak.

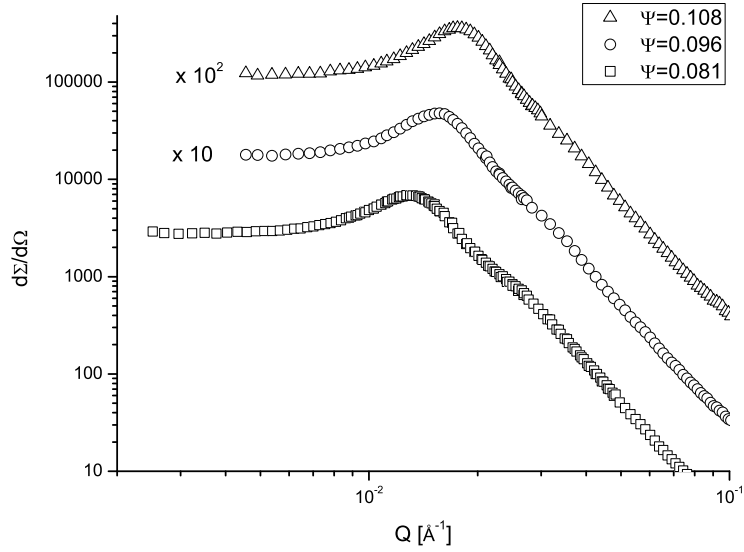


Figure 6.9: Three scattering curves for a system with changing surfactant but constant polymer amount. The upper curves are multiplied by 10 and 100 for easier comparison.

Using these simple relations we can compare the three scattering curves. The scattering vector at the peak Q_{max} seems to increase with larger surfactant amount. A larger surfactant amount leads to a higher surface to volume fraction Ψ which has to result in a decrease of the domain size. Since $d \approx (2\pi)/Q_{max}$ a decrease of the domain size results in an increase of the scattering vector of the peak, Q_{max} .

A more detailed interpretation of the scattering functions can be obtained from the earlier discussed Teubner-Strey-formula (eq. 4.21). By fitting a curve of the form

$$\frac{d\Sigma}{d\Omega}(Q) \sim \frac{1}{a - bQ^2 + cQ^4} \quad (6.1)$$

we can extract the domain size d and the correlation length ξ by comparing (6.1) with the Teubner-Strey-formula and receive:

$$k_0 = \frac{1}{2} \sqrt{2 \sqrt{\frac{a}{c}} + \frac{b}{c}} \quad (6.2)$$

$$d = \frac{2\pi}{k_0} \quad (6.3)$$

$$\xi = \frac{2}{\sqrt{2 \sqrt{\frac{a}{c}} - \frac{b}{c}}} \quad (6.4)$$

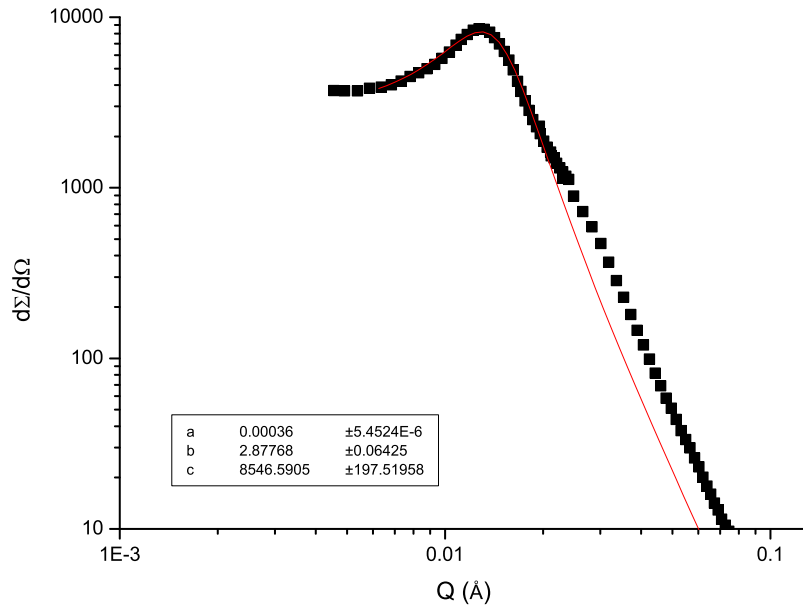


Figure 6.10: A scattering curve with the corresponding fit of the Teubner-Strey-formula. The resolution correction (chapter 4.2.2) of the experiment is included.

Figure 6.10 shows a scattering curve with the corresponding fit of the Teubner-Strey-formula. For high Q -values this fit deviates from the measure values. That is because the Teubner-Strey-formula does not account for fluctuations at much smaller length scales than the domain size of the system.

The domain size in dependence of the surface to volume fraction

We will now discuss the domain size d in dependence of the surface to volume fraction Ψ for the polymer $C_{12}E_{90}$ at different polymer concentrations δ (Figure 6.11). The domain

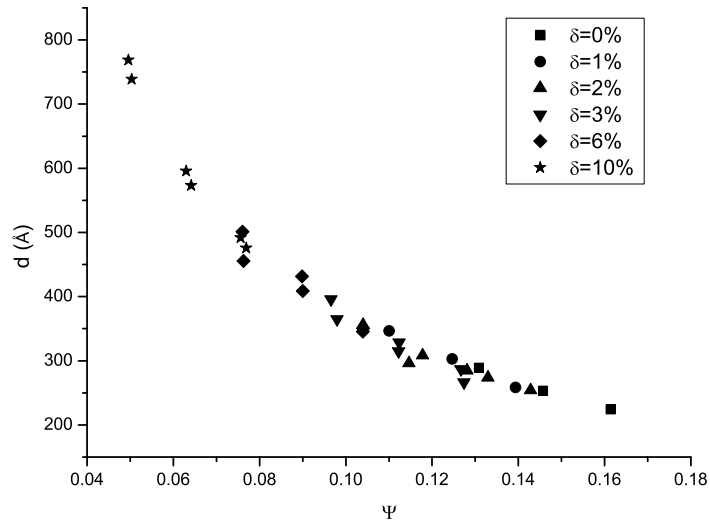


Figure 6.11: The domain size d in dependence of the surface to volume fraction Ψ for measurements with the polymer $C_{12}E_{90}$.

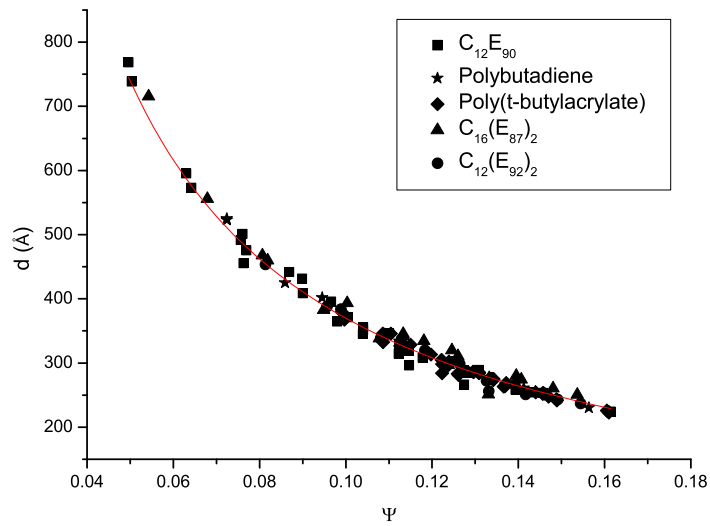


Figure 6.12: d in dependence of Ψ for all investigated polymers. The equation $d = 37\text{\AA} \cdot \Psi^{-1}$ describes this dependence.

size d decreases with the addition of surfactant. This decrease seems to be independent of the polymer amount and is therefore only characterized by the surface to volume fraction.

Figure 6.12 shows a similar plot, this time including all investigated sticker polymers. Once again, the amount and the type of the polymer have no effect on the domain size. Roux *et al.* [20] have calculated this dependence on Ψ based on a model introduced by Helfrich [21]. The basic approach $d = (2a/\Psi)$ describes a lamellar structure without fluctuations and only depends on the thickness of the surfactant interface $a \approx 12\text{\AA}$. Corrections due to short-wave fluctuations induce an additional factor:

$$d = \frac{2a}{\Psi} \left(1 + \frac{1}{4\pi} \frac{k_B T}{\kappa} \ln \left(c \sqrt{\frac{\kappa}{k_B T} \frac{d}{2\sqrt{A}}} \right) \right) \quad (6.5)$$

$A \approx 54\text{\AA}^2$ is the area of one surfactant molecule at the interface and $c = 1.84$ a constant for the practical cut-off. Assuming $d = 251\text{\AA}$ and $\kappa/k_B T = 0.42$ to be constant (legitimate due to the weak logarithmic dependence on these parameters) and $a = 12\text{\AA}$ this equation leads to $d = 3.2a/\Psi = 38\text{\AA}/\Psi$. A fit of $d = m \cdot \Psi^{-1}$ to the data gives $m = 37\text{\AA}$. The same result has been obtained in earlier measurements [13].

The correlation length in dependence of the surface to volume fraction

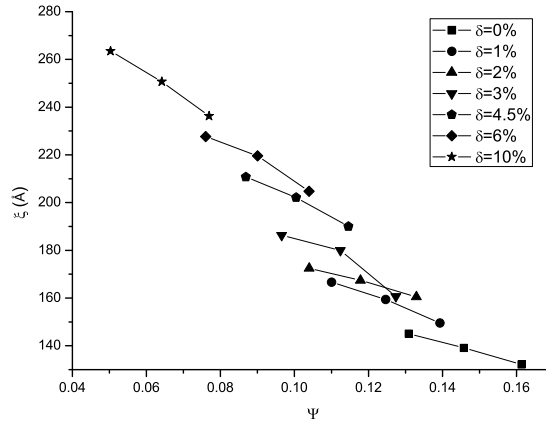


Figure 6.13: The correlation length ξ against the surfactant amount Ψ with different concentrations of the polymer $C_{12}E_{90}$.

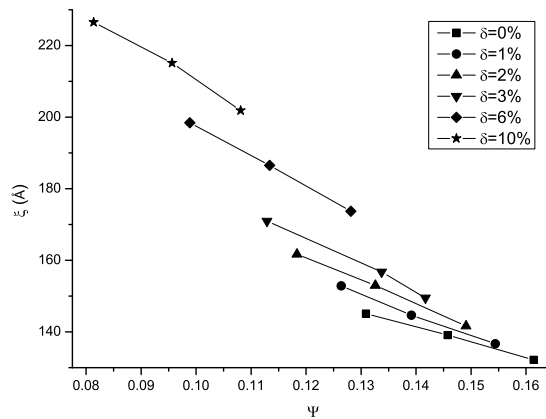


Figure 6.14: ξ in dependence of Ψ for the polymer $C_{12}(E_{92})_2$.

Figures 6.13 and 6.14 show the correlation length against Ψ for different polymer concentration. Two effects can be observed: In the first place as the surface to volume fraction gets larger the correlation length decreases. This is apparent since the domain size decreases. Second, the correlation length increases with the addition of polymers. This can be explained with the earlier discussed effect of the addition of sticker polymers to a microemulsion which suppresses fluctuations of the membrane. For a flabby interface correlated points lie close to each other whereas the correlation length is increased for a flattened interface.

Chapter 7

Discussion

After a description of the experimental work we will now take a closer look at the obtained data and carry out a more profound analysis. First we will discuss the earlier described dependence of $\ln(\Psi)$ on the scaled polymer amount σR_{ee}^2 and compare our results with the theoretical predictions. After that we discuss the influence of the polymers on the spontaneous curvature. Both information were taken from the phase diagram measurements. The last subject of this chapter will be the change of the bending rigidity evoked by the polymers which has been directly measured with small angle neutron scattering.

7.1 Efficiency boosting

We will first consider the non-ionic sticker polymers. Figure 7.1 shows $\ln(\Psi)$ against σR_w^2 . Ψ was determined from the fish-tail point of the system and σ can be calculated with equation (2.16). Even though $C_{16}(E_{87})_2$ has two hydrophilic parts, σR_w^2 shows the same dependence on the volume fraction of the polymer δ . For the bifunctional sticker polymers σ represents the density of polymer **arms** at the interface and R_w is the typical size of a single arm.

As we have discussed in chapter 3.1.1 we expect a linear dependence:

$$\ln(\Psi) = -\frac{4\pi}{\bar{\alpha}} \frac{\bar{\kappa}_0}{k_B T} - \hat{\Xi} \sigma R_w^2 \quad (7.1)$$

The predicted slope $\hat{\Xi} = -(4\pi)/\bar{\alpha} \cdot 1/6$ contains two theoretical assumptions: the first part, $(4\pi)/\bar{\alpha}$ with $\bar{\alpha} = -10/3$, arises from renormalization group calculations whereas the factor $1/6$ comes from the predicted influence of sticker polymers. Joining both

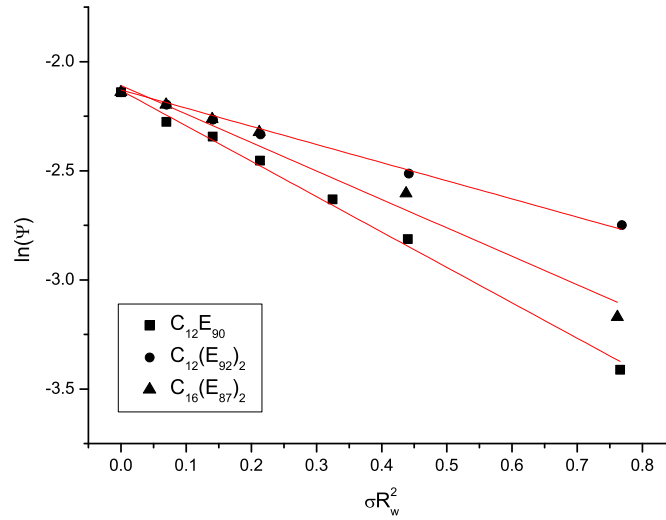


Figure 7.1: $\ln(\Psi)$ in dependence of σR_w^2 . A linear behavior with a slope of $\pi/5$ is predicted by theory.

effects we expect a slope of $\hat{\Xi} = \pi/5 = 0.628$ for ideal polymer chains. We are not able to separate the two effects when comparing this value with our results.

After a linear fit on the data we get the measured slope $\hat{\Xi}$. For the monofunctional sticker $\hat{\Xi} = 1.62 \pm 0.05$. The bifunctional sticker polymer shows a little less boosting: $\hat{\Xi} = 1.30 \pm 0.06$ for the long sticker (C_{16}) and only $\hat{\Xi} = 0.83 \pm 0.03$ for the short sticker (C_{12}). In general the phase diagrams show a bigger sensitivity to the addition of polymers as predicted by theory. This trend is a confirmation of measurements performed for the diblock copolymer which gave the result $\hat{\Xi} = 1.54 \pm 0.05$ [2]. While our measurements for the monofunctional sticker agree well with the results obtained for diblock copolymers, the consistent discrepancy to the theory might be caused by two different suppositions: an oversimplified treatment of real polymer chains and the state of the microemulsions which is assumed to be lamellar for the prediction but forms a bicontinuous structure in reality. The sensitivity of the bifunctional longer sticker polymer nearly agrees with the measurements for the monofunctional sticker, tiny amounts of polymer might still be non-active. Opposed to that the bifunctional polymer with the short sticker shows only half the sensitivity. This result is in agreement with our tendency that, due to the short sticker, some of the added polymers are not active at the interface and dissolved in the water domains as unimers. Even though the sticker has the same length as that of the monofunctional polymer, the entropic force exerted on the sticker by two hydrophilic polymer arms is larger and requires an appropriate counter-force which can be obtained by synthesizing longer stickers.

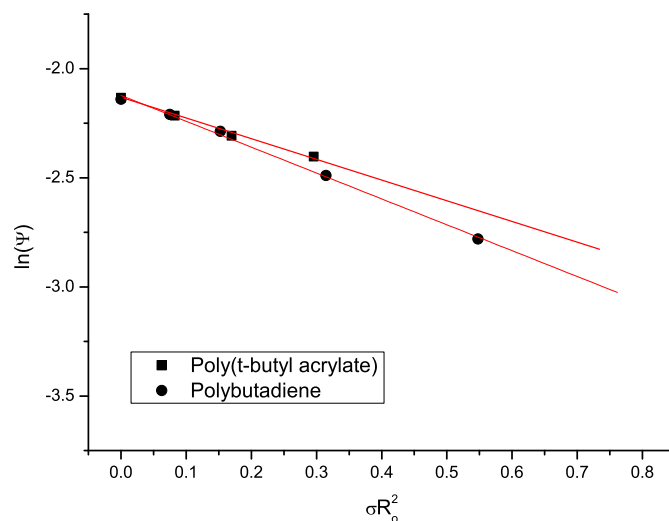


Figure 7.2: $\ln(\Psi)$ in dependence of σR_0^2 for the two ionic sticker polymers.

Figure 7.2 shows $\ln(\Psi)$ against σR_0^2 for the two ionic sticker polymers. We only compare the data taken for a pH-value of 13. The sensitivity of the first polymer, monocarboxy terminated poly(t-butyl acrylate), on $\ln(\Psi)$ is $\hat{\Xi} = 0.95 \pm 0.03$. For the addition of monocarboxy terminated polybutadiene we get $\hat{\Xi} = 1.19 \pm 0.04$.

Both ionic sticker polymers show a lower sensitivity than the two non-ionic polymers discussed earlier. These results were quite surprising since the mixture of ionic (polymer) and non-ionic (surfactant) materials has shown to lead to an increased efficiency. There might be unconsidered charge effects that influence the behavior of the polymer at the interface. Comparing the ionic polymers among each other we see a higher sensitivity for polybutadiene. This slight difference could be induced by electrostatic effects of the free Na^+ particles. Their positive charge might pull the sticker further into the water domains since the surfactant layer is tightly packed and does not allow charges to penetrate. This forces hydrophobic parts of the polymer chains into the surfactant and water domain. This unfavorable situation has a negative effect on the free energy of the polymer. Since we are dealing with an end effect, the polymer with the shorter chain, COOH-poly(t-butyl acrylate), is influenced stronger by this negative effect. Additionally, the bigger size of the monomers, and therefore a bigger volume of hydrophobic substance in water, exposes another penalty for COOH-poly(t-butyl acrylate). Last of all, the short polymer might not be a Gaussian chain.

7.2 Spontaneous curvature

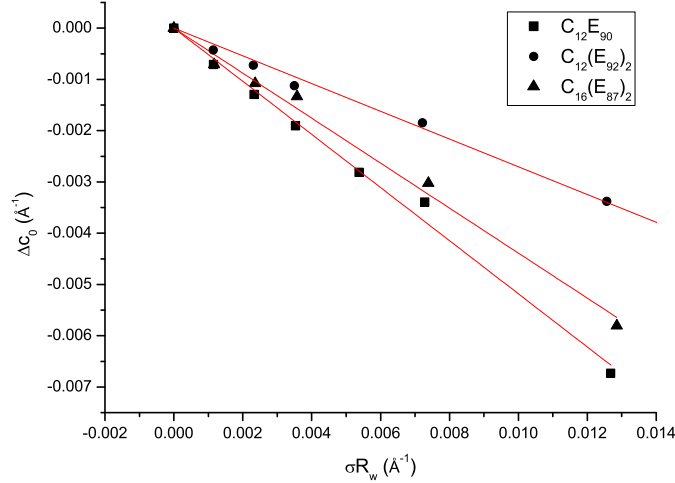


Figure 7.3: The change of the spontaneous curvature in dependence of σR_w for the three non-ionic sticker polymers.

In chapter 3.1.1 we have shown that the influence of polymers on the spontaneous curvature can be extracted from phase diagram measurements by the change of the temperature \tilde{T} . We have seen in eq. (3.3) that this change scales linear with the polymer amount σR_{ee} :

$$\Delta c_0(T) = \mp \frac{1}{4} \sqrt{\frac{\pi}{6}} \frac{k_B T}{\kappa} \sigma R_{ee} \quad (7.2)$$

The sign of Δc_0 depends on the type of the polymeric part and is negative for sticker polymers with hydrophilic chains. Approximating $\kappa/(k_B T) \approx 0.42$ (assuming a weak absolute dependence of κ on the polymer amount) gives a theoretical prediction of $\mp 1/4 \cdot \sqrt{\pi/6} \cdot (k_B T)/\kappa = \mp 0.43$ for the sensitivity of the spontaneous curvature on σR_{ee} .

Figure 7.3 shows Δc_0 against the scaled polymer amount σR_w for the non-ionic sticker polymers C₁₂E₉₀ and C₁₆(E₈₇)₂. A linear fit gives the slope $c_{slope} = -0.52 \pm 0.01$ for the monofunctional sticker polymer and $c_{slope} = -0.44 \pm 0.01$ for the bifunctional polymer with the longer sticker. The value $c_{slope} = -0.27 \pm 0.01$ for the bifunctional polymer with the short sticker relates to the fact that only part of these polymers is active at the interface. We also note that the values for the active polymers agree reasonably well with

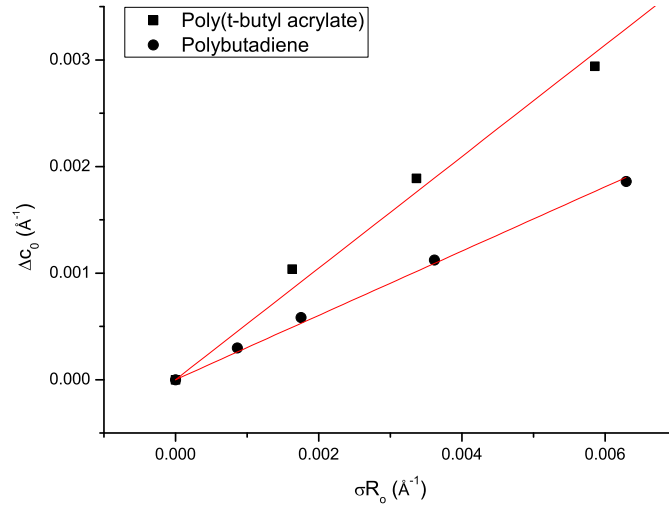


Figure 7.4: Δc_0 against σR_0 for the two ionic sticker polymers COOH-poly(t-butyl acrylate) and COOH-polybutadiene (both at pH 13).

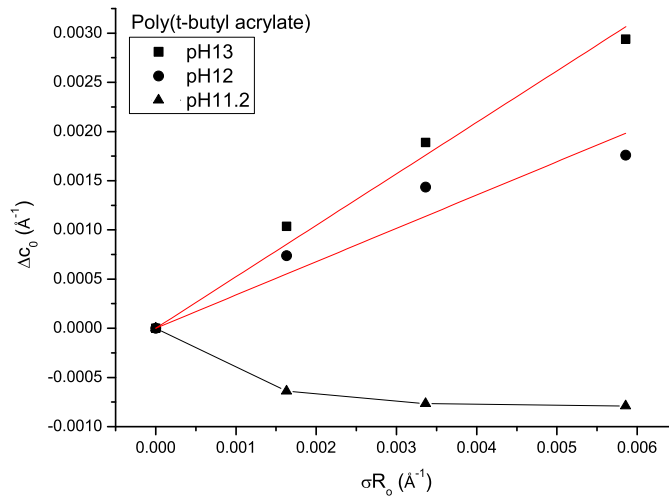


Figure 7.5: Δc_0 against σR_0 for COOH-poly(t-butyl acrylate) at all three investigated pH-values.

the theoretical prediction. The bifunctional sticker shows little less sensitivity compared to the monofunctional sticker. A possible explanation is that the entropic force of the bifunctional sticker, which bends the curvature towards oil domains, is not as strong since two polymer arms are fixed to one position (the sticker) on the membrane. Placing both arms further apart with a separate sticker for each arm has an overall stronger influence on the curvature, hence a larger sensitivity for the monofunctional sticker polymers.

Figure 7.4 shows the same plot for the two ionic sticker polymers at pH 13. This time the spontaneous curvature increases with the addition of polymers since they are only active in the oil domains and cause a curvature towards the water domains. The slopes read 0.52 ± 0.02 for COOH-poly(*t*-butyl acrylate) and 0.30 ± 0.01 for COOH-polybutadiene.

Comparing the three measurements at different pH values for COOH-poly(*t*-butyl acrylate) (figure 7.5) we see a decreased influence on the spontaneous curvature with lower pH-values. This could be interpreted by a lower activity at the interface since less NaOH is available to dissociate the ionic sticker in the water domains. The fact that the spontaneous curvature even decreases with the addition of polymers (which corresponds to a curvature towards oil domains) for the lowest allocation at pH 11.2 rises doubts about this interpretation. A possible explanation of these results will be given in context of the behavior of the bending rigidity.

7.3 Bending rigidity

We will now discuss the change of the bending rigidity induced by the addition of the different sticker polymers. It was shown in eq. (2.19) that κ depends on the surfactant amount Ψ and the scaled polymer amount σR_w^2 :

$$\frac{\kappa_R}{k_B T} = \frac{\kappa_0}{k_B T} + \frac{\alpha}{4\pi} \ln(\Psi) \Big|_{\Psi=\text{const}} + \Xi \sigma R_w^2 \quad (7.3)$$

The theoretical value is $\Xi = (1 + \pi/2)/12 \approx 0.214$. At the same time we have seen in chapter 4.3.1 that the bending rigidity is connected to the domain size d and the correlation length ξ by equation (4.15). This means that we are able to directly calculate $\kappa/k_B T$ from the data obtained by SANS measurement and gives us the possibility to compare the sensitivity of the bending rigidity on the scaled polymer amount.

Figure 7.6 shows the measured bending rigidity in units of $k_B T$ for the polymer C₁₆(E₈₇)₂. In order to only examine the influence of the polymer we compare $\kappa/k_B T$

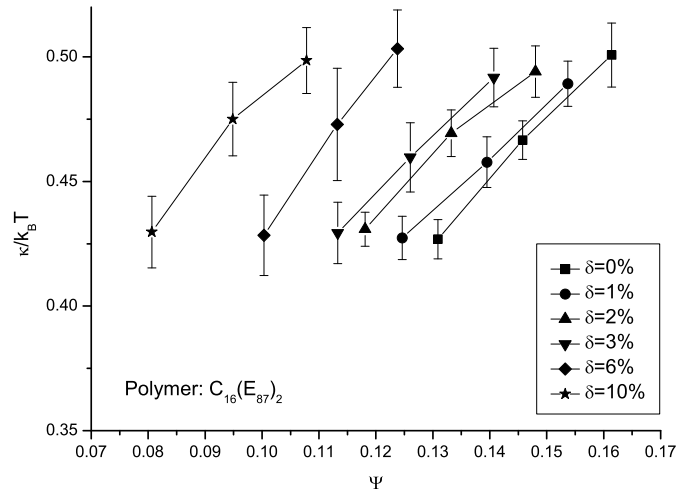


Figure 7.6: Bending rigidity κ measured by SANS in dependence of Ψ . κ is measured in units of $k_B T$, the investigated sticker polymers is $C_{16}(E_{87})_2$.

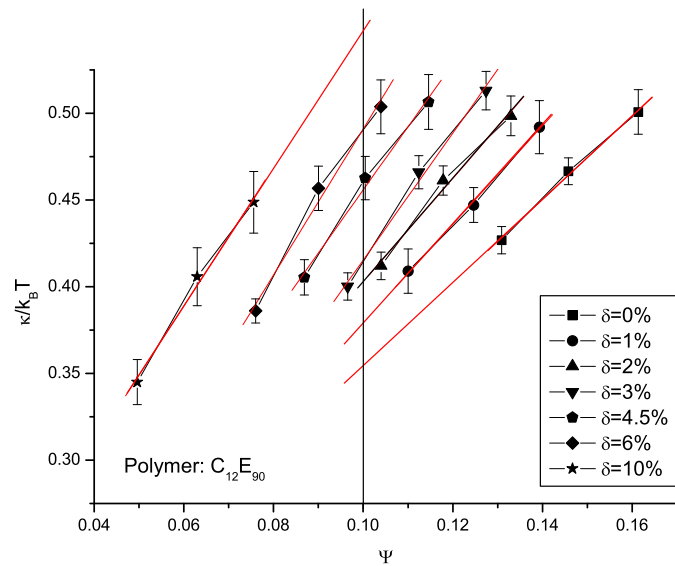


Figure 7.7: $\kappa/k_B T$ for $C_{12}E_{90}$. To investigate the influence of the polymer and eliminate the dependence of Ψ the data is extrapolated to a fixed value of $\Psi = 0.1$.

for a fixed value of Ψ . That is the reason why we have measured three different surfactant concentrations for every polymer concentration δ . Using these three measurements we are able to extrapolate the dependence on Ψ as can be seen in figure 7.7. Since any fixed value for Ψ can be chosen we pick the median of all investigated surfactant concentrations to minimize the error generated by the extrapolation of the data.

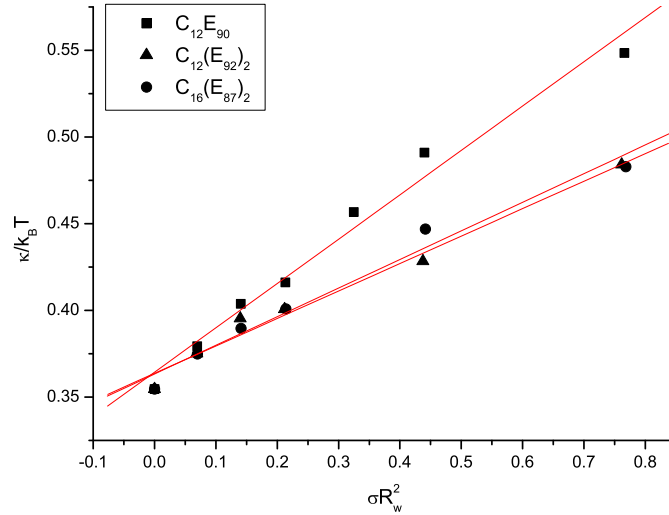


Figure 7.8: $\kappa/k_B T$ for the non-ionic sticker polymers in dependence of the scaled polymer amount σR_w^2 .

Figure 7.8 shows this dependence for all three non-ionic sticker polymers. $C_{12}E_{90}$ shows the strongest impact on the bending rigidity as was already indicated by the intense boosting effect of this polymer. A linear fit gives a sensitivity of $\Xi = 0.256 \pm 0.016$. The two bifunctional sticker polymers clearly show a weaker influence on κ . For $C_{12}(E_{92})_2$ the sensitivity is $\Xi = 0.165 \pm 0.012$ and for $C_{16}(E_{87})_2$ we get $\Xi = 0.158 \pm 0.011$.

Measurements on diblock copolymers performed by Hitoshi Endo have given a slope of 0.334. The monofunctional sticker polymers comes close to this value but are not quite as effective. This means that one diblock copolymer with two polymer chains pressing on the membrane from both sides shows a stronger influence than two sticker polymers that are only able to affect the interface from the hydrophilic side. The fact that both bifunctional polymers with different sticker lengths show an almost equal behavior regarding the effect on κ is quite surprising. Especially since the phase behavior, the influence on $\bar{\kappa}$ and that on c_0 indicated that a fraction of these polymers, in particular for the short sticker, is not active at the interface. Even the direct comparison of the raw scattering data at equal surfactant and polymer concentrations (figure 7.9) shows no significant difference.

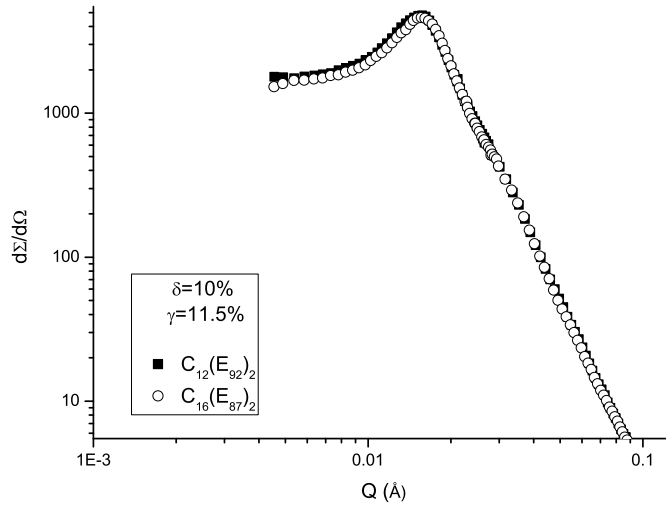


Figure 7.9: Comparison of the scattering curves for the polymers $C_{12}(E_{92})_2$ and $C_{16}(E_{87})_2$ at the same concentration of surfactant (γ) and polymer (δ).

Comparing the diblock copolymer, the monofunctional sticker polymer and the bifunctional sticker polymer we see that all three show a similar sensitivity on the saddle-splay modulus $\bar{\kappa}$ and the spontaneous curvature c_0 (for the two asymmetric polymers). Opposed to that the influence on κ clearly decreases. Computer simulations realized by Auth [22] provide an explanation of this effect: the asymmetric sticker polymers preferably anchor at the buckles of the membrane undulations that are initially induced by the surfactant. In this position the polymer coil has a reduced influence on the membrane which is reflected by a decreased sensitivity of the bending rigidity κ . The influence of this effect is even increased for bifunctional sticker polymers.

We will now discuss the influence of the two ionic sticker polymers on κ . Figure 7.10 shows the results of the SANS measurements for COOH-poly(t-butyl acrylate) at a pH-value of 11.2. We have already seen in the discussion of the phase diagrams (chapter 6.1.2) that there is just enough NaOH in the system to allow a polymer amount of $\delta = 3\%$ to attach to the interface. This result is confirmed by the SANS measurements which clearly show that the increase of δ above 3% does not influence the bending rigidity much further.

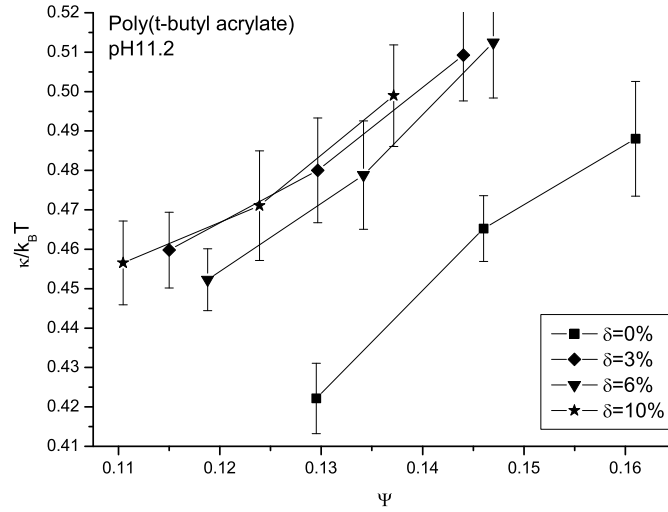


Figure 7.10: Increase of κ with the addition of COOH-poly(t-butyl acrylate) at a pH-value of 11.2. An increase of δ above 3% has no further influence.

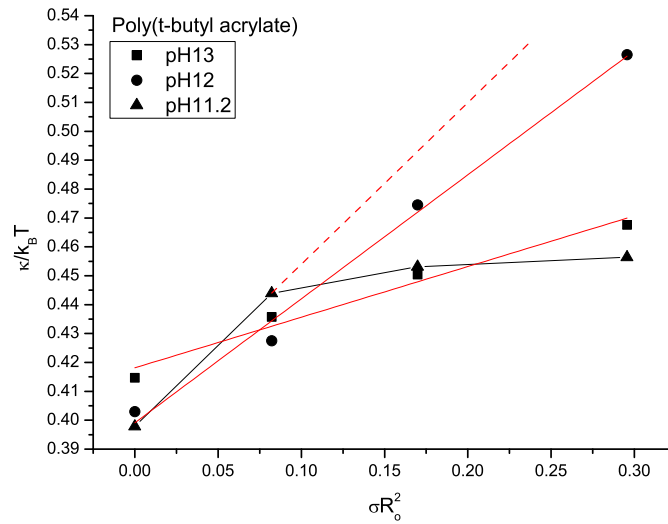


Figure 7.11: Influence of COOH-poly(t-butyl acrylate) on κ depending on the allocation.

Figure 7.11 shows the increase of $\kappa/k_B T$ with σR_o^2 for all three measured pH-values. As we have just seen the dependence flattenes for a pH-value of 11.2. Using the slope between the first two measured points (dashed red line) we get $\Xi = 0.560$ for the sensitivity. For a pH-value of 12 the sensitivity of κ on the scaled polymer amount is $\Xi = 0.429 \pm 0.027$. For ten times the amount of NaOH (pH 13) we get $\Xi = 0.175 \pm 0.019$.

A decreased sensitivity with increased pH-value is against a first expectation because a higher allocation would assure a better activity of the polymers at the interface and therefore be accompanied by an increased sensitivity of κ . To explain the effect we have to account for the free Na^+ particles available in the water domains. The COOH-sticker will release an H^+ and be left with a negative charge. Free Na^+ particles will move in and form a cloud around the negative sticker. The Debye-Hückel theory describes the electrostatic interaction of ions in electrolytes and allows to approximate the radius of this sphere:

$$R = \sqrt{\frac{2N_A e^2 I}{\epsilon k_B T}} \quad (7.4)$$

where I is the ionic strength of the available NaOH. For the highest amount of NaOH available (pH 13) the radius is $\approx 1\text{\AA}$. In this configuration plenty of Na^+ ions are available per COO^- and move very close to the negative charge. For pH 11.2 we get $R \approx 10\text{\AA}$. Thus the interaction zone diameter (20\AA) becomes comparable in size with a polymer of diameter $R_o = 70\text{\AA}$. We assume that these charged clouds press on the interface just like a polymer chain would do. This explains the decrease of the sensitivity for the spontaneous curvature with decreased pH value as we have seen in figure 7.5: As less NaOH is available, the radius of the cloud around the sticker increases and starts to balance the effect of the hydrophobic polymer that influences the other side of the membrane. At the same time it affects the membrane from two sides, similar to a diblock copolymer, and shows a stronger influence on κ with decreased pH-value.

To conclude, for the ionic sticker polymers we have found that an increase of the pH value corresponds to a decrease of the effect induced by the charge cloud until it vanishes for a pH value of 13. At the same time we have to consider the end effect which pulls part of the hydrophobic chain into the water domains and induces a decrease of the available free energy.

When comparing the influence of the two ionic sticker polymers at equal pH-value on κ (figure 7.12) we find $\Xi = 0.175 \pm 0.019$ for COOH-poly(t-butyl acrylate) and $\Xi = 0.182 \pm 0.015$ for COOH-polybutadiene. Both have equal influence on the bending rigidity.

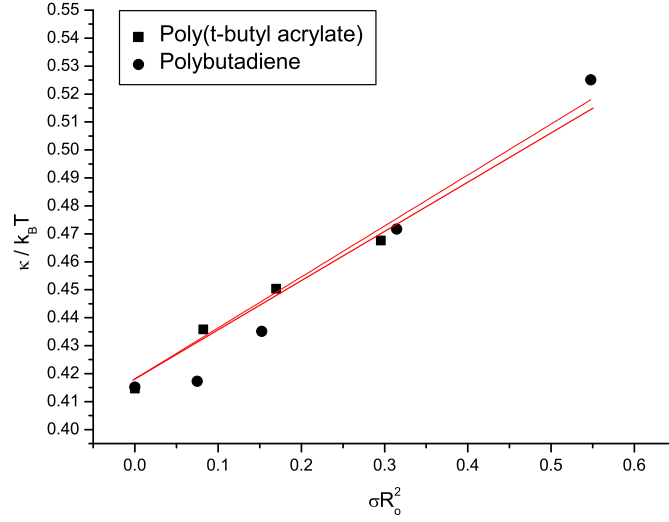


Figure 7.12: Influence of the two ionic sticker polymers on κ at equal pH values of 13.

Polymer	$\hat{\Xi}$	C_{slope}	Ξ
$C_{12}E_{90}$	1.62 ± 0.05	-0.52 ± 0.01	0.256 ± 0.016
$C_{12}(E_{92})_2$	0.83 ± 0.03	-0.27 ± 0.01	0.165 ± 0.012
$C_{16}(E_{87})_2$	1.30 ± 0.06	-0.44 ± 0.01	0.158 ± 0.011
COOH-poly(t-butyl acrylate) pH 13	0.95 ± 0.03	0.52 ± 0.02	0.175 ± 0.019
COOH-poly(t-butyl acrylate) pH 12	-	0.339 ± 0.034	0.429 ± 0.027
COOH-poly(t-butyl acrylate) pH 11.2	-	-0.40	0.560
COOH-polybutadiene	1.19 ± 0.04	0.30 ± 0.01	0.182 ± 0.015

Table 7.1: Summary of all results for the five investigated polymers.

Chapter 8

Summary and conclusions

In this work we aimed to replace amphiphilic diblock copolymers by sticker polymers as efficiency boosters in microemulsions. These polymers have a short hydrophobic sticker and a long hydrophilic polymeric block or vice versa. Efficiency boosting describes the significantly lower amount of surfactant needed to solubilize equal amounts of water and oil. We studied monofunctional stickers of the $C_{12}E_{90}$ type in comparison to equivalent diblock copolymers. Bifunctional sticker polymers were interesting because their behavior is less flexible with respect to the anchoring point. Since the anchoring was not stable for a $C_{12}(E_{92})_2$ sticker, we had to extend the study to a $C_{16}(E_{87})_2$ sticker with a better anchor. The ionic stickers reverse the amphiphilicity, which might be interesting for applications in which the domains of the droplets are reversed. The current studies focus on bicontinuous microemulsions.

Using the measured phase diagrams, we were able to determine the minimum amount of surfactant necessary to solubilize all available water and oil at the phase inversion temperature \tilde{T} . A comparison of these values for different polymer concentrations allowed us to evaluate the change of the saddle splay modulus $\bar{\kappa}$ and the spontaneous curvature c_0 depending on the scaled polymer amount. The domain size d and the correlation length ξ were obtained from SANS experiments using the Teubner-Strey formula to describe the distribution of scattered neutrons. The Gaussian random field model links d and ξ with the bending rigidity κ . Therefore SANS allows us to directly measure the influence of polymers on κ .

We have summarized our results in one plot comparing the theoretical predictions, measurements on the diblock copolymer [2] and our measurements on the sticker polymers. Figure 8.1 shows the coefficients $\hat{\Xi}$, c_{slope} and Ξ , which measure the sensitivity of $\bar{\kappa}$, c_0 and κ as a function of the scaled polymer amount on a logarithmic scale. For $\hat{\Xi}$ we notice a discrepancy (factor two) between the theoretical predictions and the measured data. The oversimplified treatment of the polymer branches as ideal chains and the assumption of a lamellar instead of a bicontinuous domain structure are most probably

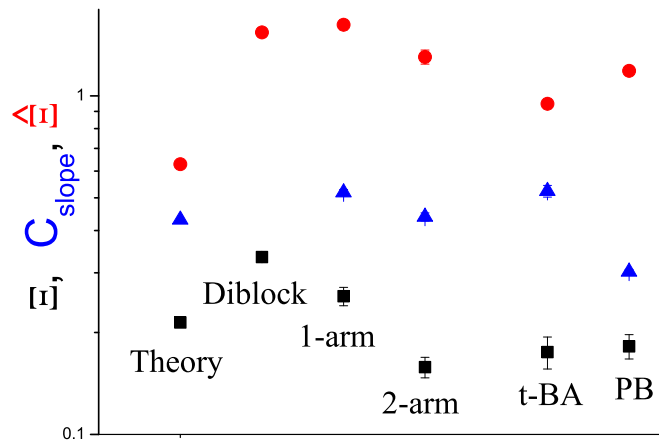


Figure 8.1: Summary of the results for the theoretical prediction, diblock copolymer [2], the monofunctional sticker polymer, the bifunctional sticker polymer (longer sticker) and the two ionic sticker polymers COOH-poly(*t*-butyl acrylate) and COOH-polybutadiene at pH 13.

responsible for the deviation.

We have successfully shown that non-ionic sticker polymers in microemulsions can be used as efficiency boosters. The influence on $\bar{\kappa}$ shows a similar sensitivity as was found for diblock copolymers. The slightly decreased impact of the bifunctional sticker polymers might be due to a reduced activity at the interface. Both hydrophilic arms exert an entropic force on the sticker and try to pull it out of the membrane. The impact on the spontaneous curvature shows a similar trend: the sensitivity of the bifunctional sticker is slightly decreased compared to the monofunctional sticker. The diblock copolymer shows no change of c_0 due to its symmetric structure. In contrast to these results we observe a clear decrease for the sensitivity of κ . Simulations by Auth [22] suggest that the asymmetric sticker polymers prefer to position themselves at buckles of the fluctuating surfactant membrane. The effect on κ is therefore reduced for monofunctional sticker polymers and, particularly, for bifunctional sticker polymers.

We have also investigated two ionic sticker polymers which are active in the oil domains of the microemulsion. NaOH was added to the system to allow the COOH-sticker to dissociate in the water domains. Their different influence on the saddle-splay modulus was explained with the effect caused by the positive Na^+ charges available in the water domains (both measurements were performed at pH 13). The charges pull the COO^- sticker and with it parts of the hydrophobic polymer chain into the water domains, which has a negative influence on the free energy. This end effect will have a smaller influence

on polybutadiene since it has four times more monomers than poly(t-butyl acrylate). We also noticed a smaller impact on the spontaneous curvature.

To determine the role of the Na^+ allocation, three different pH values were investigated for COOH-poly(t-butyl acrylate). We noticed a strong decrease for the sensitivity on κ with increased pH value. This was explained by Na^+ charge clouds that form around the electronegative sticker and influence the membrane. As the pH value is increased, more positive particles are available and the size of the charge cloud decreases. Since the latter has a similar effect as a hydrophilic polymer coil, its positive effect is reduced. This concept is supported by measurements of the spontaneous curvature induced by the charge clouds.

We have shown that sticker polymers can be used as efficiency boosters as they are similarly effective as diblock copolymers. Bifunctional sticker polymers might need an even longer sticker to guarantee complete activity at the interface. In future, it will be interesting to investigate star polymers with more than one hydrophilic and hydrophobic arm since they will not follow the undulations of the surfactant film. To fully understand ionic sticker polymers, more measurements at different pH values have to be carried out.

Chapter 9

Bibliography

- [1] B. Jakobs, *Langmuir* **15**, 6707 (1999).
- [2] H. Endo, M. Mihailescu, M. Monkenbusch, J. Allgaier, G. Gompper, D. Richter, B. Jakobs, T. Sottmann, R. Strey and I. Grillo, *J. Chem. Phys.*, **115**, 580 (2001)
- [3] W. Helfrich, *Z. Naturforsch.* **28c**, 693XS (1973).
- [4] M. Teubner and R. Strey, *J. Chem. Phys.*, **87**, 3195 (1987).
- [5] R. Strey, *J. Colloid Polm. Sci.* **272**, 1005 (1994).
- [6] L. Peliti and S. Leibler, *Phys. Rev. Lett.*, **54**, 1690 (1985).
- [7] D. C. Morse, *Phys. Rev.*, E **50**, R2423 (1994).
- [8] G. Gompper, in *33. IFF-Ferienkurs: Soft Matter*, Forschungszentrum Jülich GmbH, Jülich, 1991, Kap. B9.
- [9] C. Hiergeist and R. Lipowsky, *J. Phys. II France*, **6**, 1465 (1996).
- [10] S. T. Milner and T. A. Witten, *J. Phys. France*, **49**, 1951 (1988).
- [11] E. Eisenriegler, A. Hanke and S. Dietrich, *Phys. Rev.*, E **54**, 1134 (1996).
- [12] Sottmann T., *Dissertation*, Georg-August-Universität zu Göttingen, Göttingen, 1997.
- [13] D. Byelov, *Dissertation*, Westfälische Wilhelms-Universität Münster, Münster, 2003.
- [14] D. Richter, in *Laboratory Course Neutron Scattering*, Forschungszentrum Jülich GmbH, Jülich, 2005, chapter 2.

- [15] J. S. Pedersen D. Posselt and K. Mortensen, *J. Appl. Cryst.*, **23**, 321 (1990).
- [16] P. Pieruschka and S. A. Safran, *Europhysics Letters*, **22**, 625 (1993).
- [17] C. Frank, *Dissertation*, Universität zu Köln, Köln, 2004.
- [18] M. Kahlweit and R. Strey, *Angew. Chem. Int. Ed. Engl.*, **24**, 654 (1985)
- [19] M. Kahlweit, R. Strey and P. Firman, *J. Phys. Chem.*, **90**, 671 (1986)
- [20] D. Roux, F. Nallet, E. Freyssingeas, G. Porte, P. Bassereau, M. Skouri and J. Marignan, *Europhysics Letters*, **17**, 575 (1992).
- [21] W. Helfrich, *Z. Naturforsch.*, A **33**, 305 (1978).
- [22] Auth T. and Gompper G., *Phys. Rev. E* **72**, 31904 (2005).

Acknowledgements

I would like to thank Prof. Dr. D. Richter and Prof. Dr. T. Brückel for the chance to write my diploma thesis at the IFF of Research Centre Juelich, for their guidance and for their kind support. It has been a great pleasure working in such a highly professional and encouraging environment.

As to detailed advice and practical support, I am first and foremost indebted to Dr. H. Frielinghaus. Apart from professional considerations, I enjoyed the personal dimension of cooperation.

Futhermore, I would also like to thank Prof. G. Gompper for the theoretical interpretation of results and for fruitful discussions.

I am grateful to Dr. J. Allgaier and Dr. L. Willner for the synthesis of the investigated polymers and the support of the work in the laboratory.

Likewise, I am grateful to Dr. G. Mangiapia, who supported me during the first measurements at KWS2 and Dr. C. Frank for the introduction to phase diagram measurements.

On the whole, the warm reception by the staff of IFF provided a pleasant working atmosphere.

I appreciate the linguistic support I received from my father, Heinz Brodeck, who proof-read the paper.

Last but not least, I would like to thank my family and the Hagner family, especially Anne, for their mental support.